Parameter sensitivity analysis of dynamic ice sheet models

Preprint · June 2019

CITATIONS
0

READS
18

2 authors:

Gong Cheng
Uppsala University
14 PUBLICATIONS **42** CITATIONS
SEE PROFILE

Per Lötstedt
Uppsala University
121 PUBLICATIONS **2,396** CITATIONS
SEE PROFILE

PARAMETER SENSITIVITY ANALYSIS OF DYNAMIC ICE SHEET MODELS *

GONG CHENG† AND PER LÖTSTEDT†

Abstract. The velocity and the height at the surface of a dynamic ice sheet are observed. The ice sheets are modeled by the full Stokes, SIA and SSA equations. The sensitivity of the observed quantities at the ice surface to parameters in the models, e.g. the base topography and friction coefficients, is analyzed by first deriving the time dependent adjoint equations. Using the adjoint solutions, the effect of a perturbation in a parameter is obtained. The adjoint equations are solved analytically and numerically and the sensitivity is determined in several examples in two dimensions.

Key words. ice sheet modeling, inverse problem, adjoint method, sensitivity analysis

AMS subject classifications. 86A40, 86A22, 35R30, 76D07

1. Introduction.

In computational models for the flow of ice in glaciers and continental ice sheets, it is necessary to choose models and supply parameters for the sliding between the ice base and the bedrock. Direct observations of the basal conditions by drilling holes in the ice are not feasible except for a few locations. Instead, the data for the sliding models are inferred from observations of the surface elevation and velocity of the ice from aircraft and satellites, see e.g. [18, 29]. How to do this is an important question because the basal sliding is a key uncertainty in the assessment of the future sea level rise due to melting ice [25].

The flow of ice is well modeled by the full Stokes (FS) equations, see [6]. They form a system of partial differential equations (PDEs) for the stress and pressure in the ice with a nonlinear viscosity coefficient. The domain of the ice is confined by an upper surface and a bottom either resting on the bedrock or floating on sea water. The boundary conditions at the upper surface of the ice and at the floating part are well defined. For the ice in contact with the bedrock, a friction model with parameters determines the sliding force. The sliding depends e.g. on the topography at the ice base, the friction between the ice and the bedrock, and the meltwater under the ice. The upper, free boundary of the ice and the interface between the ice and water are advected by equations for the height and the interface.

The computational effort to solve the FS equations is quite large and there is often a need for approximations. The FS equations are simplified by integrating in the depth of the ice in the shallow shelf (or shelfy stream) approximation (SSA) [6, 15]. The spatial dimension of the problem is reduced by one with SSA compared to FS. The shallow ice approximation (SIA) is a good approximation in the inner parts of an ice sheet where vertical shear stresses dominate over the longitudinal stresses in the ice flow [6, 37].

*Submitted to the editors 2019-06-20.

Funding: This work was funded by FORMAS 2017-00665

†Division of Scientific Computing, Department of Information Technology, Uppsala University, P. O. Box 337, SE-75105 Uppsala, Sweden (cheng.gong@it.uu.se, per.lotstedt@it.uu.se).

The friction law is often of Weertman type [36] but other friction models are also considered [33]. The model for the relation between the sliding speed and the pressure and the friction at the bed is discussed in [19, 31]. It is not clear how to formulate a relation that is generally applicable. When the parameters in the sliding model in the forward equation are unknown but data are available such as the surface velocity and elevation of the ice, an inverse problem is solved by minimizing the distance between the observations and the predictions of the PDE model with the parameters. The gradient of the objective function for the minimization is computed by solving an adjoint equation as in [1, 38]. With a fixed thickness of the ice, the adjoint of the FS equation is derived in [24] and for SSA with a frozen viscosity in [16].

The basal parameters are estimated from uncertain observational data at the surface in [4, 12] and initial data for ice sheet simulations are found in [23] using the same technique as in [24]. The sensitivity of the ice flow to the basal conditions is investigated in [10] with the adjoint solution. Part of the drag at the base may be due to the resolution of the topography. The geometry at the ice base is inferred by an inversion method in [22]. The difficulty in separating the topography from the sliding properties at base in the inversion is also addressed in [14, 32]. Considerable differences in the friction coefficient in the FS and SSA models are found after inversion in [26]. By linearization of the model equations, a transfer operator is derived in [7, 8] and it is shown in [9] how the topography and the friction coefficients are affected by measurement errors at the surface.

It is noted in [34] that the friction coefficient varies in space and time. The time scales of the variations are diurnal [28], seasonal [30], and decennial [13]. The time it takes for the surface to respond to sudden changes in basal conditions are determined analytically and numerically in [8] with SIA, SSA, and FS. These papers indicate that it is not sufficient to infer the friction parameters from the time-independent adjoint to the FS stress equation but to include also the time dependent height advection equation in the inversion.

In this paper, we study how perturbations in the sliding conditions and the topography at the base of the ice are affecting observations of the height of the ice and the velocity at the surface for the FS, SIA, and SSA models. The friction law is due to Weertman [36]. The sensitivity to perturbations of the parameters in FS and SSA is determined by solving an adjoint problem of the same kind as for inverse problems with a fixed ice thickness in [16, 24]. The difference here is that the adjoint of the time dependent advection equation for the height is also solved allowing height observations and the influence is evaluated of the adjoint height in the adjoint solution. The adjoint equations follow from the Lagrangian of the forward equations after partial integration. Analytical solutions to the adjoint equations are determined in two dimensions (2D) under simplifying but reasonable assumptions making the dependence of parameters explicit. The sensitivity in SIA solutions is found algebraically without solving differential equations. Conclusions are drawn in the final section. Extensive numerical computations are reported in a companion paper [2].

2. Ice models. The full Stokes equations in glaciology are system of nonlinear PDEs for the flow of ice on the ground and ice floating on water [6]. The nonlinearity is due to the viscosity of the ice according to Glen's flow law [5]. The ice is assumed to be isothermal and obeys a friction law at the contact surface between the ice and the bedrock. The upper surface of the ice is a moving boundary and satisfies an evolution

equation for the height of the ice. In the SIA and the SSA equations, the low aspect ratio of an ice-sheet/shelf, i.e. the thickness scale divided by the length scale, is used to simplify the FS equations.

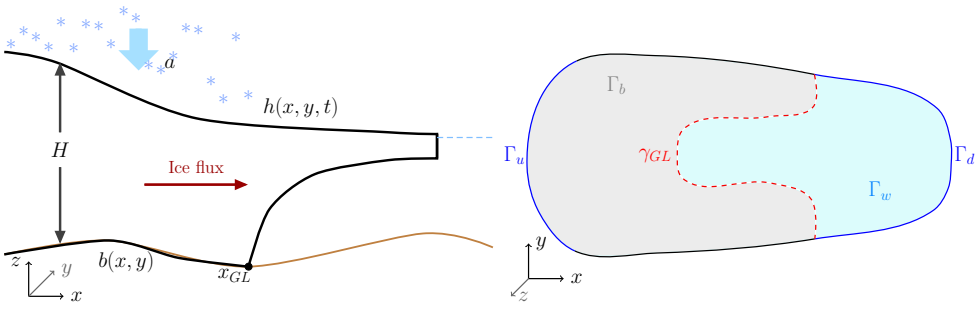

FIG. 1. *A schematic view of an ice sheet in the $x-z$ (left panel) and $x-y$ (right panel) plane. The grounding line is at $x = x_{GL}$. Left: The upper surface Γ_s is at $z = h(x, y, t)$, the grounded boundary Γ_b is at $z = z_b(x, y, t) = b(x, y)$ for $x < x_{GL}$, and the floating boundary Γ_w at $z = z_b(x, y, t)$ for $x > x_{GL}$. Right: The grounded part of the base is Γ_b and the floating part is Γ_w separated by the grounding line γ_{GL}.*

2.1. Full Stokes equation. Let u_1, u_2, and u_3 be the velocity components of $\mathbf{u} = (u_1, u_2, u_3)^T$ in the x, y and z directions and $\mathbf{x} = (x, y, z)^T$ in three dimensions (3D). Vectors and matrices are written in bold characters. The horizontal plane is spanned by the x and y coordinates and z is the coordinate in the vertical direction. Let the subscript x, y, z or t denote a derivative with respect to the variable. The height of the upper surface is $h(x, y, t)$, the z coordinates of the bedrock and the floating interface are $b(x, y)$ and $z_b(x, y, t)$, and the ice thickness is $H = h - b$, as shown in Figure 1.

The strain rate $\mathbf{D}$ and the viscosity η are given by

$$\mathbf{D}(\mathbf{u}) = \tfrac{1}{2}(\nabla\mathbf{u} + \nabla\mathbf{u}^T),\ \eta(\mathbf{u}) = \tfrac{1}{2}A^{-\frac{1}{n}}(\mathrm{tr}\mathbf{D}^2(\mathbf{u}))^{\nu},\ \nu = \tfrac{1-n}{2n}, \tag{2.1}$$

where $\mathrm{tr}\mathbf{D}^2$ is the trace of $\mathbf{D}^2$. The rate factor A in (2.1) is dependent on the temperature and Glen's flow law determines $n > 0$, here taken to be $n = 3$. The stress tensor is

$$\boldsymbol{\sigma}(\mathbf{u}, p) = 2\eta\mathbf{D}(\mathbf{u}) - \mathbf{I}p, \tag{2.2}$$

where p is the pressure and $\mathbf{I}$ is the identity matrix. The domain occupied by the ice is Ω with boundary Γ whose outward pointing normal is $\mathbf{n}$. If $\mathbf{x} \in \Omega$ then $(x, y) \in \omega$ in the $x - y$ plane. The upper boundary is Γ_s at the ice surface. The vertical, lateral boundary has an upstream part Γ_u where $\mathbf{n} \cdot \mathbf{u} \le 0$ and a downstream part Γ_d where $\mathbf{n} \cdot \mathbf{u} > 0$. The lower boundary at the bedrock is Γ_b and the floating boundary is Γ_w. They are separated by the grounding line γ_{GL} defined by $(x_{GL}(y), y)$ by assuming the ice mainly flows along the x-axis. If $\mathbf{x} \in \Gamma_u$ or $\mathbf{x} \in \Gamma_d$ then $(x, y) \in \gamma_u$ or $(x, y) \in \gamma_d$ where $\gamma = \gamma_u \cup \gamma_d$ is the boundary of ω. The definitions of these domains are

$$\begin{aligned}
\Omega &= \{\mathbf{x} | (x, y) \in \omega,\ b(x, y) \le z \le h(x, y, t)\},\\
\Gamma_s &= \{\mathbf{x} | (x, y) \in \omega,\ z = h(x, y, t)\},\\
\Gamma_b &= \{\mathbf{x} | (x, y) \in \omega,\ z = b(x, y),\ x < x_{GL}(y)\},\\
\Gamma_w &= \{\mathbf{x} | (x, y) \in \omega,\ z = z_b(x, y, t),\ x > x_{GL}(y)\},\\
\Gamma_u &= \{\mathbf{x} | (x, y) \in \gamma_u,\ b(x, y) \le z \le h(x, y, t)\},\\
\Gamma_d &= \{\mathbf{x} | (x, y) \in \gamma_d,\ b(x, y) \le z \le h(x, y, t)\},
\end{aligned} \tag{2.3}$$

and a schematic view in the $x-y$ plane is shown in the right panel of Figure 1.

In two dimensions (2D), $\mathbf{x} = (x, z)^T$, $\omega = [0, L]$, $\gamma_u = 0$, and $\gamma_d = L$ where L is the horizontal length of the domain.

The basal stress on Γ_b is related to the basal velocity using an empirical friction law. The friction coefficient has a general form $\beta(\mathbf{u}, \mathbf{x}, t) = C(\mathbf{x}, t)f(\mathbf{u})$ where the coefficient $C(\mathbf{x}, t)$ is independent of the velocity $\mathbf{u}$ and $f(\mathbf{u})$ represents some linear or nonlinear functions of $\mathbf{u}$. For instance, $f(\mathbf{u}) = \|\mathbf{u}\|^{m-1}$ with the norm $\|\mathbf{u}\| = (\mathbf{u}\cdot\mathbf{u})^{1/2}$ introduces a Weertman type friction law [36] on ω with a Weertman friction coefficient $C(\mathbf{x}, t) > 0$ and an exponent parameter $m > 0$. Common choices of m are 1/3 and 1.

The density of the ice is denoted by ρ, the accumulation/ablation rate on Γ_s by a, and the gravitational acceleration by $\mathbf{g}$. A projection [24] on the tangential plane of Γ_b is denoted by $\mathbf{T} = \mathbf{I} - \mathbf{n} \otimes \mathbf{n}$ where the Kronecker outer product between two vectors $\mathbf{a}$ and $\mathbf{c}$ or two matrices $\mathbf{A}$ and $\mathbf{C}$ is defined by

$$(\mathbf{a} \otimes \mathbf{c})_{ij} = a_i c_j, \quad (\mathbf{A} \otimes \mathbf{C})_{ijkl} = A_{ij} C_{kl}. \tag{2.4}$$

With $\mathbf{h} = (h_x, h_y, -1)^T$ (in 2D $\mathbf{h} = (h_x, -1)^T$), the forward equations for the height and velocity are

$$\begin{aligned}
&h_t + \mathbf{h} \cdot \mathbf{u} = a, \ \text{ on } \Gamma_s,\\
&h(\mathbf{x}, 0) = h_0(\mathbf{x}), \ \mathbf{x} \in \omega, \quad h(\mathbf{x}, t) = h_\gamma(\mathbf{x}, t), \ \mathbf{x} \in \gamma_u,\\
&-\nabla \cdot \boldsymbol{\sigma}(\mathbf{u}, p) = -\nabla \cdot (2\eta(\mathbf{u})\mathbf{D}(\mathbf{u})) + \nabla p = \rho \mathbf{g}, \quad \nabla \cdot \mathbf{u} = 0, \ \text{in } \Omega(t),\\
&\boldsymbol{\sigma}\mathbf{n} = \mathbf{0}, \ \text{on } \Gamma_s,\\
&\mathbf{T}\boldsymbol{\sigma}\mathbf{n} = -Cf(\mathbf{T}\mathbf{u})\mathbf{T}\mathbf{u}, \quad \mathbf{n} \cdot \mathbf{u} = 0, \ \text{on } \Gamma_b,
\end{aligned} \tag{2.5}$$

where $h_0(\mathbf{x})$ is the initial height and $h_\gamma(\mathbf{x}, t)$ is a given height on the inflow boundary. The boundary conditions of the velocity on Γ_u and Γ_d are of Dirichlet type such that

$$\mathbf{u}|_{\Gamma_u} = \mathbf{u}_u, \quad \mathbf{u}|_{\Gamma_d} = \mathbf{u}_d, \tag{2.6}$$

where $\mathbf{u}_u$ and $\mathbf{u}_d$ are some known velocities. In a special case where Γ_u is at the ice divide, the horizontal velocity is set to $\mathbf{u}|_{\Gamma_u} = \mathbf{0}$, and the vertical component of $\boldsymbol{\sigma}\mathbf{n}$ also vanishes on Γ_u.

2.2. Shallow shelf approximation. On the ice shelf and the fast flowing region, the basal shear stress is negligibly small and the horizontal velocity is almost constant in the z direction [6, 15, 27]. The 3D FS problem (2.5) on Ω can be simplified to a 2D problem with $\mathbf{x} = (x, y) \in \omega$ by SSA, where only the horizontal velocity components $\mathbf{u} = (u_1, u_2)^T$ are considered. The viscosity for the SSA is

$$\eta(\mathbf{u}) = \frac{1}{2}A^{-\frac{1}{n}}\left(u_{1x}^2 + u_{2y}^2 + \frac{1}{4}(u_{1y} + u_{2x})^2 + u_{1x}u_{2y}\right)^{\nu} = \frac{1}{2}A^{-\frac{1}{n}}\left(\frac{1}{2}\mathbf{B} : \mathbf{D}\right)^{\nu}, \tag{2.7}$$

and the vertically integrated stress tensor $\boldsymbol{\varsigma}(\mathbf{u})$ is defined as

$$\boldsymbol{\varsigma}(\mathbf{u}) = 2H\eta\mathbf{B}(\mathbf{u}), \tag{2.8}$$

where $\mathbf{B}(\mathbf{u}) = \mathbf{D}(\mathbf{u}) + \nabla \cdot \mathbf{u}\,\mathbf{I}$ with $\nabla \cdot \mathbf{u} = \operatorname{tr}\mathbf{D}(\mathbf{u})$. The Frobenius inner product between two matrices $\mathbf{A}$ and $\mathbf{C}$ is defined by

$$\mathbf{A} : \mathbf{C} = \sum_{ij} A_{ij}C_{ij}. \tag{2.9}$$

Let $\mathbf{n}$ be the outward normal vector of the boundary $\gamma = \gamma_u \cup \gamma_d$ and $\mathbf{t}$ the tangential vector such that $\mathbf{n} \cdot \mathbf{t} = 0$. The friction law is defined as in the FS case where the basal velocity is replaced by the horizontal velocity since the vertical variation is neglected in SSA. An example is Weertman's law defined by $\beta(\mathbf{u}, \mathbf{x}, t) = C(\mathbf{x}, t) f(\mathbf{u}) = C(\mathbf{x}, t) \|\mathbf{u}\|^{m-1}$ with a friction coefficient $C(\mathbf{x}, t) \geq 0$. In Figure 1, $\omega = \Gamma_b \cup \Gamma_w$ and $\gamma_u = \Gamma_u$, $\gamma_d = \Gamma_d$.

The ice dynamics system is

$$
\begin{array}{l}
h_t + \nabla \cdot (\mathbf{u} H) = a, \;\; 0 \leq t \leq T, \; \mathbf{x} \in \omega, \\
h(\mathbf{x}, 0) = h_0(\mathbf{x}), \; \mathbf{x} \in \omega, \quad h(\mathbf{x}, t) = h_\gamma(\mathbf{x}, t), \; \mathbf{x} \in \gamma_u, \\
\nabla \cdot \boldsymbol{\varsigma} - C f(\mathbf{u}) \mathbf{u} = \rho g H \nabla h, \; \mathbf{x} \in \omega, \\
\mathbf{n} \cdot \mathbf{u}(\mathbf{x}, t) = u_u(\mathbf{x}, t), \mathbf{x} \in \gamma_u, \quad \mathbf{n} \cdot \mathbf{u}(\mathbf{x}, t) = u_d(\mathbf{x}, t), \mathbf{x} \in \gamma_d, \\
\mathbf{t} \cdot \boldsymbol{\varsigma} \mathbf{n} = -C_\gamma f_\gamma(\mathbf{t} \cdot \mathbf{u}) \mathbf{t} \cdot \mathbf{u}, \; \mathbf{x} \in \gamma_g, \quad \mathbf{t} \cdot \boldsymbol{\varsigma} \mathbf{n} = 0, \; \mathbf{x} \in \gamma_w.
\end{array} \tag{2.10}
$$

The inflow and outflow normal velocities $u_u \leq 0$ and $u_d > 0$ are specified on γ_u and γ_d. The lateral side of the ice γ is split into γ_g and γ_w with $\gamma = \gamma_g \cup \gamma_w$. There is friction in the tangential direction on γ_g which depends on the tangential velocity $\mathbf{t} \cdot \mathbf{u}$ with the friction coefficient C_γ and relation f_γ. The structure of the SSA system (2.10) is similar to the FS equations in (2.5). However, the velocity $\mathbf{u}$ is not divergence free in SSA and $\mathbf{B} \neq \mathbf{D}$ due to the cryostatic approximation of p.

In the case where an ice shelf or a grounding line exists, the floating ice is assumed to be at hydrostatic equilibrium in the seawater. A calving front boundary condition [27, 35] is applied at γ_d by the depth integrated stress balance

$$
\boldsymbol{\varsigma}(\mathbf{u}) \cdot \mathbf{n} = \frac{1}{2} \rho g H^2 \left(1 - \frac{\rho}{\rho_w} \right) \mathbf{n}, \; \mathbf{x} \in \gamma_d, \tag{2.11}
$$

where ρ_w is the density of seawater. With this boundary condition, a calving rate u_c can be determined at the ice front.

2.3. Shallow ice approximation. For the area far away from the ice domes and the grounding line, the shear stress in the horizontal plane dominates the ice flow. A first order approximation of FS can be made by neglecting the shear stress in the vertical plane and the normal deviatoric stress based on the hydrostatic approximation [11, 20]. The length scales in the vertical and the horizontal directions, H and L, vary by orders of magnitude for a continental ice sheet such that $\varepsilon = H/L \sim 10^{-2} - 10^{-3}$. This fact is utilized when the SIA equations are derived.

Assuming that the rate factor A of the ice sheet is constant, the horizontal velocities u_1, u_2 and the volume flux $\mathbf{Q}$ can be written in a closed form as

$$
\begin{aligned}
\begin{pmatrix} u_1(\mathbf{x}, t) \\ u_2(\mathbf{x}, t) \end{pmatrix} &= -C_b (\rho g H)^{\theta - \lambda} \|\nabla h\|^{\theta - 1} \nabla h \\
&\quad - \tfrac{2}{n+1} A (\rho g)^n \|\nabla h\|^{n-1} \nabla h (H^{n+1} - (h - z)^{n+1}), \\
\mathbf{Q}(x, y, t) &= \begin{pmatrix} Q_1 \\ Q_2 \end{pmatrix} = \int_b^h \begin{pmatrix} u_1(\mathbf{x}, t) \\ u_2(\mathbf{x}, t) \end{pmatrix} dz \\
&= -C_b (\rho g H)^{\theta - \lambda} H \|\nabla h\|^{\theta - 1} \nabla h - \tfrac{2}{(n+2)} A (\rho g)^n \|\nabla h\|^{n-1} \nabla h H^{n+2},
\end{aligned} \tag{2.12}
$$

where $C_b \geq 0$ is the basal sliding coefficient with a different interpretation than the friction coefficient C in (2.5) and θ and λ are the sliding exponents. Depending on the

base conditions, (θ, λ) are for example $(3,2), (3,1)$ and $(1,0)$ [6]. In this formulation, the volume flux is locally determined by the surface gradient ∇h and the thickness of the ice H. The height evolution is governed by an equation similar to the height equation in (2.5)

$$\begin{aligned} &h_t + \nabla \cdot \mathbf{Q} = a, \ \ 0 \le t \le T, \ \mathbf{x} \in \omega, \\ &h(\mathbf{x}, 0) = h_0(\mathbf{x}), \ \mathbf{x} \in \omega, \quad h(\mathbf{x}, t) = h_\gamma(\mathbf{x}, t), \ \mathbf{x} \in \gamma_u, \end{aligned} \tag{2.13}$$

assuming that $b(x, y)$ is constant in time. Replacing the volume flux $\mathbf{Q}$ by (2.12), the dynamics of the ice sheet under SIA is modeled by a nonlinear PDE (2.13) for the unknown $h(x, y, t)$.

3. Adjoint equations. We wish to determine the sensitivity of a functional

$$\mathcal{F} = \int_0^T \int_{\Gamma_s} F(\mathbf{u}, h) \, \mathrm{d}\mathbf{x} \, \mathrm{d}t \tag{3.1}$$

to perturbations in the friction coefficient $C(\mathbf{x}, t)$ at the base of the ice and the topography $b(\mathbf{x})$ when $\mathbf{u}$ and h satisfy the FS equations (2.5) or the SSA equations (2.10). We introduce a Lagrangian $\mathcal{L}(\mathbf{u}, p, h; \mathbf{v}, q, \psi; b, C)$ for a given observation $\mathcal{F}$ with the forward solution $(\mathbf{u}, p, h)$ to (2.5) or $(\mathbf{u}, h)$ to (2.10) and the corresponding adjoint solutions $(\mathbf{v}, q, \psi)$ or $(\mathbf{v}, \psi)$. The adjoint solutions solve the adjoint equations to the FS and SSA equations. These equations will be derived using the Lagrangian in this section and Appendix A.

The effect of the perturbations δC and δb in C and b on $\mathcal{F}$ is given by the perturbation $\delta\mathcal{L}$ in the Lagrangian

$$\begin{aligned} \delta\mathcal{F} \ &= \delta\mathcal{L} \\ &= \mathcal{L}(\mathbf{u} + \delta\mathbf{u}, p + \delta p, h + \delta h; \mathbf{v} + \delta\mathbf{v}, q + \delta q, \psi + \delta\psi; b + \delta b, C + \delta C) \\ &\quad -\mathcal{L}(\mathbf{u}, p, h; \mathbf{v}, q, \psi; b, C). \end{aligned}$$

Examples of $F(\mathbf{u}, h)$ in (3.1) are $\|\mathbf{u} - \mathbf{u}_{\text{obs}}\|^2$, $|h - h_{\text{obs}}|^2$ in an inverse problem to find b and C to match the observed data $\mathbf{u}_{\text{obs}}$ and h_{obs} at the surface Γ_s as in [4, 12, 21, 24], or $F(\mathbf{u}, h) = \frac{1}{T} u_1(\mathbf{x}, t) \delta(\mathbf{x} - \mathbf{x}_*)$ with the Dirac delta at $\mathbf{x}_*$ to measure the time averaged deviation of the horizontal velocity u_1 at $\mathbf{x}_*$ on the ice surface Γ_s with

$$\mathcal{F} = \int_0^T \int_{\Gamma_s} F(\mathbf{u}, h) \, \mathrm{d}\mathbf{x} \, \mathrm{d}t = \frac{1}{T} \int_0^T u_1(\mathbf{x}_*, t) \, \mathrm{d}t.$$

The duration of the observation is determined by T.

3.1. Full Stokes equation. The definition of the Lagrangian $\mathcal{L}$ for the FS equations is found (A.15) in Appendix A where $(\mathbf{v}, q, \psi)$ are the Lagrange multipliers corresponding to the forward equations for $(\mathbf{u}, p, h)$. In order to determine $(\mathbf{v}, q, \psi)$, the so-called adjoint problem is solved

$$\begin{aligned} &\psi_t + \nabla \cdot (\mathbf{u}\psi) - \mathbf{h} \cdot \mathbf{u}_z \psi = F_h + F_{\mathbf{u}} \cdot \mathbf{u}_z, \ \ \text{on } \Gamma_s, \\ &\psi(\mathbf{x}, T) = 0, \ \psi(\mathbf{x}, t) = 0, \ \text{on } \Gamma_d, \\ &-\nabla \cdot \tilde{\boldsymbol{\sigma}}(\mathbf{v}, q) = -\nabla \cdot (2\tilde{\boldsymbol{\eta}}(\mathbf{u}) \star \mathbf{D}(\mathbf{v})) + \nabla q = \mathbf{0}, \quad \nabla \cdot \mathbf{v} = 0, \ \text{in } \Omega(t), \\ &\tilde{\boldsymbol{\sigma}}(\mathbf{v}, q)\mathbf{n} = -(F_{\mathbf{u}} + \psi\mathbf{h}), \ \text{on } \Gamma_s, \\ &\mathbf{T}\tilde{\boldsymbol{\sigma}}(\mathbf{v}, q)\mathbf{n} = -Cf(\mathbf{Tu}) \left(\mathbf{I} + \mathbf{F}_b(\mathbf{Tu})\right) \mathbf{Tv}, \ \text{on } \Gamma_b, \\ &\mathbf{n} \cdot \mathbf{v} = 0, \ \text{on } \Gamma_b, \end{aligned} \tag{3.2}$$

where the derivatives of F with respect to $\mathbf{u}$ and h are

$$F_{\mathbf{u}} = \left(\frac{\partial F}{\partial u_1}, \frac{\partial F}{\partial u_2}, \frac{\partial F}{\partial u_3}\right)^T, \quad F_h = \frac{\partial F}{\partial h}.$$

The adjoint viscosity and adjoint stress [24] are

$$\begin{aligned} \tilde{\boldsymbol{\eta}}(\mathbf{u}) &= \eta(\mathbf{u})\left(\mathcal{I} + \tfrac{1-n}{n\mathbf{D}(\mathbf{u}):\mathbf{D}(\mathbf{u})}\mathbf{D}(\mathbf{u}) \otimes \mathbf{D}(\mathbf{u})\right), \\ \tilde{\boldsymbol{\sigma}}(\mathbf{v}, q) &= 2\tilde{\boldsymbol{\eta}}(\mathbf{u}) \star \mathbf{D}(\mathbf{v}) - q\mathbf{I}. \end{aligned} \tag{3.3}$$

The tensor $\mathcal{I}$ has four indices $ijkl$ and $\mathcal{I}_{ijkl} = 1$ only when $i = j = k = l$ and 0 otherwise. In general, $\mathbf{F}_b(\mathbf{Tu})$ in (3.2) is a linearization of the friction law relation $f(\mathbf{Tu})$ in (2.5) with respect to the variable $\mathbf{Tu}$. For instance, with a Weertman type friction law, $f(\mathbf{Tu}) = \|\mathbf{Tu}\|^{m-1}$, it is

$$\mathbf{F}_b(\mathbf{Tu}) = \frac{m-1}{\mathbf{Tu}\cdot\mathbf{Tu}}(\mathbf{Tu}) \otimes (\mathbf{Tu}). \tag{3.4}$$

The $\star$ operation between a four index tensor $\mathcal{A}$ and a two index tensor or matrix $\mathbf{C}$ is defined by

$$(\mathcal{A} \star \mathbf{C})_{ij} = \sum_{kl} \mathcal{A}_{ijkl} C_{kl}. \tag{3.5}$$

The perturbation of the Lagrangian function with respect to a perturbation δC in the slip coefficient $C(\mathbf{x}, t)$ is

$$\delta\mathcal{F} = \delta\mathcal{L} = \int_0^T \int_{\Gamma_b} f(\mathbf{Tu})\mathbf{Tu}\cdot\mathbf{Tv}\ \delta C\ \mathrm{d}\mathbf{x}\,\mathrm{d}t \tag{3.6}$$

involving the tangential components of the forward and adjoint velocities $\mathbf{Tu}$ and $\mathbf{Tv}$ at the ice base Γ_b.

The detailed derivation of the adjoint equations (3.2) and the perturbation of the Lagrangian function (3.6) are given in Appendix A from the weak form of the FS equations (2.5) on Ω, integration by parts, and by applying the boundary conditions as in e.g. [17, 24]. The adjoint equations consist of the equations for the adjoint height ψ, the adjoint velocity $\mathbf{v}$, and the adjoint pressure q. Compared to the steady state adjoint equation for the FS equation in [24], an advection equation is added in (3.2) for the Lagrange multiplier $\psi(\mathbf{x}, t)$ on Γ_s with a right hand side depending on the observation function F and one term depending on ψ in the boundary condition on Γ_s. The adjoint height equation of ψ can be solved independently of the adjoint stress equation since it is independent of $\mathbf{v}$. If h is observed then the adjoint height equation must be solved together with the adjoint stress equation. Otherwise, the term $\psi\mathbf{h}$ vanishes in the right hand side of the adjoint stress equation and the solution is $\mathbf{v} = \mathbf{0}$ with $\delta\mathcal{F} = 0$ in (3.6).

3.1.1. Time-dependent perturbations. Suppose that $u_1(\mathbf{x}_*, t_*)$ is observed at (x_*, t_*) at the ice surface and that $t_* < T$, then

$$u_1(\mathbf{x}_*, t_*) = \mathcal{F} = \int_{\Gamma_s} \int_0^T F(\mathbf{u})\,\mathrm{d}\mathbf{x}\,\mathrm{d}t,$$

with

$$F(\mathbf{u}) = u_1\delta(\mathbf{x}-\mathbf{x}_*)\delta(t-t_*),\ F_{u_1} = \delta(\mathbf{x}-\mathbf{x}_*)\delta(t-t_*),\ F_{u_2} = F_{u_3} = 0,\ F_h = 0.$$

The procedure to determine the sensitivity is as follows. First solve the forward equation (2.5) forward in time for $\mathbf{u}(\mathbf{x},t)$. Then solve the adjoint equation (3.2) backward in time for $t \le T$ with $\psi(\mathbf{x},T) = 0$ as final condition. The solution for $t_* < t \le T$ is $\psi(\mathbf{x},t) = 0$ and $\mathbf{v}(\mathbf{x},t) = \mathbf{0}$. Denote the unit vector with 1 in the i:th component by $\mathbf{e}^i$. At $t = t_*$ we have

$$\tilde{\boldsymbol{\sigma}}(\mathbf{v},q)\mathbf{n} = -\mathbf{e}^1\delta(\mathbf{x}-\mathbf{x}_*)\delta(t-t_*) - \psi\mathbf{h},$$

in the boundary condition in (3.2). For $t < t_*$, $\tilde{\boldsymbol{\sigma}}(\mathbf{v},q)\mathbf{n} = -\psi\mathbf{h}$. Since ψ is small for $t < t_*$ (see subsection 3.1.3), the dominant part of the solution is $\mathbf{v}(\mathbf{x},t) = \mathbf{v}_0(\mathbf{x})\delta(t-t_*)$ for some $\mathbf{v}_0$.

When the slip coefficient is changed by δC, then the change in $u_1(\mathbf{x}_*,t_*)$ is by (3.6)

$$\begin{aligned}\delta u_1(x_*,t_*) &= \delta\mathcal{L} = \int_0^T\int_{\Gamma_b} f(\mathbf{Tu})\mathbf{Tu}\cdot\mathbf{Tv}\,\delta C\,\mathrm{d}\mathbf{x}\,\mathrm{d}t\\ &\approx \int_{\Gamma_b} f(\mathbf{Tu})\mathbf{Tu}\cdot\mathbf{Tv}_0\,\delta C(\mathbf{x},t_*)\,\mathrm{d}\mathbf{x}.\end{aligned} \tag{3.7}$$

In this case, the perturbation $\delta u_1(\mathbf{x}_*,t_*)$ only depends on δC at time t_*.

Suppose that the height $h(\mathbf{x}_*,t_*)$ is measured at Γ_s. Then

$$F(h) = h(x,t)\delta(\mathbf{x}-\mathbf{x}_*)\delta(t-t_*),\ F_h = \delta(\mathbf{x}-\mathbf{x}_*)\delta(t-t_*),\ F_{\mathbf{u}} = \mathbf{0}.$$

The solution of the adjoint equation (3.2) with $\tilde{\boldsymbol{\sigma}}(\mathbf{v},q)\mathbf{n} = -\psi\mathbf{h}$ at Γ_s for $\mathbf{v}(\mathbf{x},t)$ is non-zero since $\psi(\mathbf{x},t) \ne 0$ for $t < t_*$. In a seasonal variation, there is a time dependent perturbation $\delta C(\mathbf{x},t) = \delta C_0(\mathbf{x})\cos(2\pi t/\tau)$ added to a stationary time average $C(\mathbf{x})$. The time constant τ could be e.g. 1 year. Assume that $f(\mathbf{Tu})\mathbf{Tu}\cdot\mathbf{Tv}$ is approximately constant in time (e.g. if $\mathbf{u}$ varies slowly, then $\psi \approx$ const and $\mathbf{v} \approx$ const for $t < t_*$). Then the observation at the ice surface varies as

$$\begin{aligned}\delta h(x_*,t_*) &= \delta\mathcal{L} = \int_0^T\int_{\Gamma_b} f(\mathbf{Tu})\mathbf{Tu}\cdot\mathbf{Tv}\,\delta C(\mathbf{x},t)\,\mathrm{d}\mathbf{x}\,\mathrm{d}t\\ &\approx \int_0^{t_*}\cos(2\pi t/\tau)\,\mathrm{d}t\int_{\Gamma_b} f(\mathbf{Tu})\mathbf{Tu}\cdot\mathbf{Tv}\,\delta C_0\,\mathrm{d}\mathbf{x}\\ &= \frac{\tau}{2\pi}\sin(2\pi t_*/\tau)\int_{\Gamma_b} f(\mathbf{Tu})\mathbf{Tu}\cdot\mathbf{Tv}\,\delta C_0\,\mathrm{d}\mathbf{x}.\end{aligned} \tag{3.8}$$

When the friction perturbation δC is large at $t_* = 0, \tau/2, \tau\ldots$ the effect on $h(x_*,t_*)$ vanishes. If the middle of the winter is at $n\tau$, $n = 0,1,2,\ldots$, then the middle of the summer is at $(n+1/2)\tau$. The friction is at its maximum in the winter and at its minimum in the summer when the meltwater introduces lubrication. There is no change of $h(x_*,t_*)$ in the middle of the summer, $\delta h(x_*,t_*) = 0$, but $C+\delta C$ has its lowest value then. If $h(x_*,t_*)$ is measured in the summer and compared to a mean value $h(\mathbf{x})$, then $\delta h(\mathbf{x},t_*) = 0$ and the wrong conclusion would be drawn that there is no change in C if the phase shift between δC and δh in (3.8) is not accounted for.

A 2D numerical example is shown in Figure 2 with $\tau = 1$ year and $\delta C(x,t) = 0.01C\cos(2\pi t)$ in an interval $x \in [0.9, 1.0]\times 10^6$ m where the ice sheet flows from

$x = 0$ to $L = 1.6 \times 10^6$ m. The grounding line is at $x_{GL} = 1.035 \times 10^6$ m. The details of the setup are found in [2]. The ice sheet is simulated by FS with Elmer/Ice [3] for 10 years. The perturbations in δu_1 and δh oscillate regularly with a period of 1 year after an initial transient and are small outside the interval $[0.9, 1.0] \times 10^6$. An increase in the friction, $\delta C > 0$, leads to a decrease in the velocity and $\delta C < 0$ increases the velocity. There is a phase shift $\Delta\phi$ in time by $\pi/2$ between δu and dh as predicted by (3.7) and (3.8). The weight in (3.8) for δC_0 changes sign when the observation point is passing from $x_* = 0.9 \times 10^6$ to 1.0×10^6.

The phase shift $\Delta\phi$ between the surface observations and the basal perturbations is investigated in [7] with a linearized equation and Fourier analysis. It is found that $\Delta\phi = -\pi/2$ between δC and δh for short perturbation wave lengths in the steady state as in Figure 2.

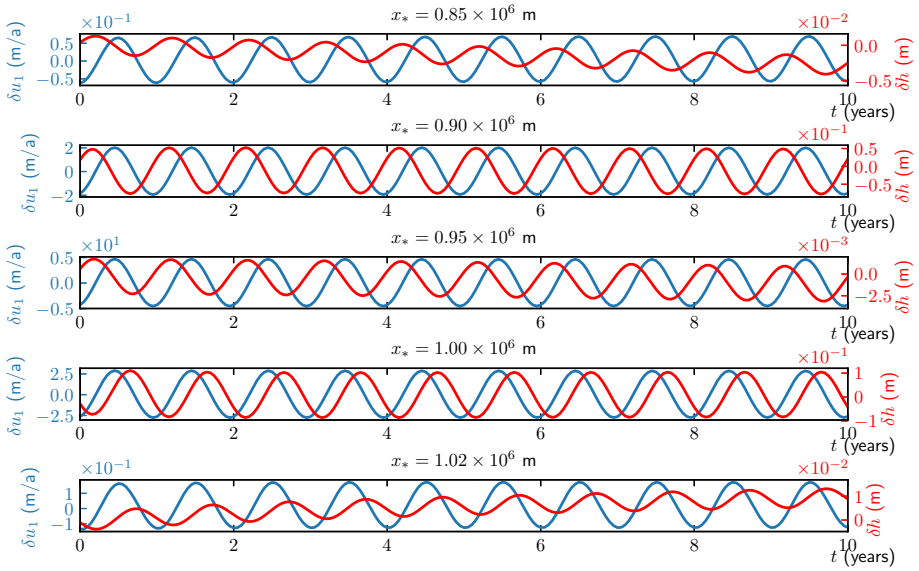

FIG. 2. *Observations at* $x_* = 0.85, 0.9, 0.95, 1.0, 1.02 \times 10^6$ *m with FS in time* $t \in [0, 10]$ *of* δu_1 *(blue) and* δh *(red) with perturbation* $\delta C(t) = 0.01C\cos(2\pi t)$ *for* $x \in [0.9, 1.0] \times 10^6$ *m.*

3.1.2. The sensitivity problem and the inverse problem. There is a relation between the sensitivity problem and the inverse problem to infer parameters from data. Assume that $(\mathbf{v}_*^i, q_*^i, \psi_*^i), i = 1, \ldots, d$, solves (3.2) with $F_\mathbf{u} = \mathbf{e}^i\delta(\mathbf{x} - \mathbf{x}_*)$ or $F_h = \delta(\mathbf{x} - \mathbf{x}_*)$. With $F_\mathbf{u} \neq 0, F_h = 0$ we have $d = 2\,(3)$ in 2D (3D) and with $F_\mathbf{u} = 0, F_h \neq 0$ we have $d = 1$. Consider a target functional $\mathcal{F}$ for the steady state solution with weights $w_i(\mathbf{x}_*)$ multiplying δu_*^i in the first variation of $\mathcal{F}$. Using (3.6), $\delta\mathcal{F}$ is

$$
\begin{aligned}
\delta\mathcal{F} &= \int_\omega \sum_{i=1}^d w_i(\mathbf{x}_*)\delta u_*^i \,\mathrm{d}\mathbf{x}_* = \int_\omega \sum_{i=1}^d w_i(\mathbf{x}_*) \int_{\Gamma_b} f(\mathbf{Tu})\mathbf{Tu}\cdot\mathbf{T}\mathbf{v}_*^i \,\delta C \,\mathrm{d}\mathbf{x}\,\mathrm{d}\mathbf{x}_* \\
&= \int_{\Gamma_b} f(\mathbf{Tu})\mathbf{Tu}\cdot\mathbf{T}\left(\int_\omega \sum_{i=1}^d w_i(\mathbf{x}_*)\mathbf{v}_*^i \,\mathrm{d}\mathbf{x}_*\right)\delta C \,\mathrm{d}\mathbf{x}.
\end{aligned} \tag{3.9}
$$

It follows from (3.2) that $(w_i(\mathbf{x}_*)\mathbf{v}_*^i(\mathbf{x}), w_i(\mathbf{x}_*)q_*^i(\mathbf{x}), w_i(\mathbf{x}_*)\psi_*^i(\mathbf{x}))$ is a solution with $F_\mathbf{u} = w_i(\mathbf{x}_*)\mathbf{e}_i\delta(\mathbf{x}-\mathbf{x}_*)$ or $F_h = w(\mathbf{x}_*)\delta(\mathbf{x}-\mathbf{x}_*)$. Therefore, also

$$\left(\int_\omega w_i(\mathbf{x}_*)\mathbf{v}_*^i\,\mathrm{d}\mathbf{x}_*, \int_\omega w_i(\mathbf{x}_*)q_*^i\,\mathrm{d}\mathbf{x}_*, \int_\omega w_i(\mathbf{x}_*)\psi_*^i\,\mathrm{d}\mathbf{x}_*\right)$$

is a solution with $F_\mathbf{u} = \int_\omega w_i(\mathbf{x}_*)\mathbf{e}^i\delta(\mathbf{x}-\mathbf{x}_*)\,\mathrm{d}\mathbf{x}_* = w_i(\mathbf{x})\mathbf{e}^i$ or $F_h = \int_\omega w(\mathbf{x}_*)\delta(\mathbf{x}-\mathbf{x}_*)\,\mathrm{d}\mathbf{x}_* = w(\mathbf{x})$.

In the inverse problem, $\mathcal{F} = \frac{1}{2}\int_\omega \|\mathbf{u}(\mathbf{x}) - \mathbf{u}_{\mathrm{obs}}(\mathbf{x})\|^2\,\mathrm{d}\mathbf{x}$ [24] and the first variation is $\delta\mathcal{F} = \int_\omega(\mathbf{u}(\mathbf{x}) - \mathbf{u}_{\mathrm{obs}}(\mathbf{x}))\cdot\delta\mathbf{u}(\mathbf{x})\,\mathrm{d}\mathbf{x}$. Let $w_i(\mathbf{x}) = u_i(\mathbf{x}) - u_{\mathrm{obs},i}(\mathbf{x})$ in (3.9). Then we find that

$$\delta\mathcal{F} = \int_{\Gamma_b} f(\mathbf{Tu})\mathbf{Tu}\cdot\mathbf{T}\tilde{\mathbf{v}}(\mathbf{x})\,\delta C\,\mathrm{d}\mathbf{x}, \tag{3.10}$$

where

$$\tilde{\mathbf{v}}(\mathbf{x}) = \int_\omega \sum_{i=1}^d w_i(\mathbf{x}_*)\mathbf{v}_*^i(\mathbf{x})\,\mathrm{d}\mathbf{x}_*$$

is a solution to (3.2) with $F_\mathbf{u} = (w_1, w_2, w_3)^T = \mathbf{u} - \mathbf{u}_{\mathrm{obs}}$ or $F_h = w = h - h_{\mathrm{obs}}$.

If we are interested in solving the inverse problem and determine $\delta\mathcal{F}$ in (3.9) to iteratively compute the optimal solution, then we solve (3.2) directly with $F_\mathbf{u} = \mathbf{u} - \mathbf{u}_{\mathrm{obs}}$ or $F_h = h - h_{\mathrm{obs}}$ to obtain $\tilde{\mathbf{v}}$ without computing $\mathbf{v}_*^i$.

3.1.3. Steady state solution to the adjoint height equation in 2D. In 2D, with $\mathbf{u}(x,z) = (u_1, u_3)^T$, the stationary equation for ψ in (3.2) is

$$(u_1\psi)_x = F_h + (\mathbf{h}\psi + F_\mathbf{u})\cdot\mathbf{u}_z,\ z = h,\ 0 \le x \le L. \tag{3.11}$$

When $x > x_*$, where $F_h = 0$ and $F_\mathbf{u} = 0$, then $\psi(x) = 0$ since the right boundary condition is $\psi(L) = 0$.

If u_1 is observed at Γ_s then $F(\mathbf{u}, h) = u_1(x)\chi(x)$ and $F_\mathbf{u} = (\chi(x), 0)^T$ and $F_h = 0$. The weight χ on u_1 may be a Dirac delta, a Gaussian, or a constant in a limited interval. On the other hand, if $F(\mathbf{u}, h) = h(x)\chi(x)$ then $F_h = \chi(x)$ and $F_\mathbf{u} = \mathbf{0}$.

Let $g(x) = u_{1z}(x)$ when $F_\mathbf{u} \neq \mathbf{0}$ and let $g(x) = 1$ when $F_h \neq 0$. Then by (3.11)

$$(u_1\psi)_x - \mathbf{h}\cdot\mathbf{u}_z\psi = g(x)\chi(x). \tag{3.12}$$

The solution to (3.12) is

$$\begin{aligned} \psi(x) &= -\frac{1}{u_1(x)}\int_x^{x_*} \exp\left(-\int_x^\xi \frac{\mathbf{h}\cdot\mathbf{u}_z(y)}{u_1(y)}\,\mathrm{d}y\right) g(\xi)\chi(\xi)\,\mathrm{d}\xi,\ 0 \le x < x_*, \\ \psi(x) &= 0,\ x_* < x \le L. \end{aligned} \tag{3.13}$$

In particular, if $\chi(x) = \delta(x - x_*)$ then $\mathcal{F} = u(x_*)$ or $\mathcal{F} = h(x_*)$ and the multiplier is

$$\psi(x) = -\frac{g(x_*)}{u_1(x)}\exp\left(-\int_x^{x_*} \frac{\mathbf{h}\cdot\mathbf{u}_z(y)}{u_1(y)}\,\mathrm{d}y\right),\ 0 \le x < x_*, \tag{3.14}$$

which has a jump $-g(x_*)/u_1(x_*)$ at x_*. With a small $\mathbf{h}\cdot\mathbf{u}_z(y) \approx 0$ above, an approximate solution is $\psi(x) \approx -g(x_*)/u_1(x)$. This may often be the case. For instance, in SIA in (2.12) $u_{1z}(x, y, h) = 0$ and in SSA by assumption $u_{1z}(x) = 0$.

3.2. Shallow shelf approximation. The adjoint equations for SSA are given and analyzed in this section. A Lagrangian $\mathcal{L}$ of the SSA equations is defined with the same technique as in [24] for the FS equations. By evaluating $\mathcal{L}$ at the forward solution $(\mathbf{u}, h)$ and the adjoint solution $(\mathbf{v}, \psi)$, the effect of perturbed data at the ice base can be observed at the ice surface as a perturbation $\delta\mathcal{L}$. The details of the derivations are found in Appendix A. In 2D steady state, the equations are simpler and analytical solutions for the forward and adjoint equations are derived later in this section.

After insertion of the forward solution, partial integration in $\mathcal{L}$, and applying the boundary conditions, the adjoint SSA equations are obtained as

(3.15)
$$\begin{aligned}
&\psi_t + \mathbf{u}\cdot\nabla\psi + 2\eta\mathbf{B}(\mathbf{u}) : \mathbf{D}(\mathbf{v}) - \rho g H\nabla\cdot\mathbf{v} + \rho g\mathbf{v}\cdot\nabla b = F_h, \quad \text{in } \omega,\\
&\psi(\mathbf{x}, T) = 0, \quad \text{in } \omega, \qquad \psi(\mathbf{x}, t) = 0, \quad \text{on } \gamma_w,\\
&\nabla\cdot\tilde{\boldsymbol{\varsigma}}(\mathbf{v}) - Cf(\mathbf{u})(\mathbf{I} + \mathbf{F}_\omega(\mathbf{u}))\mathbf{v} - H\nabla\psi = -F_{\mathbf{u}}, \quad \text{in } \omega,\\
&\mathbf{t}\cdot\tilde{\boldsymbol{\varsigma}}(\mathbf{v})\mathbf{n} = -C_\gamma f_\gamma(\mathbf{t}\cdot\mathbf{u})(1 + F_\gamma(\mathbf{t}\cdot\mathbf{u}))\mathbf{t}\cdot\mathbf{v}, \text{ on } \gamma_g, \quad \mathbf{t}\cdot\tilde{\boldsymbol{\varsigma}}(\mathbf{v})\mathbf{n} = 0, \text{ on } \gamma_w,\\
&\mathbf{n}\cdot\mathbf{v} = 0, \text{ on } \gamma,
\end{aligned}$$

where the adjoint viscosity $\tilde{\boldsymbol{\eta}}$ and adjoint stress $\tilde{\boldsymbol{\varsigma}}$ are defined by

$$\begin{aligned}
\tilde{\boldsymbol{\eta}}(\mathbf{u}) &= \eta(\mathbf{u})\left(\mathcal{I} + \tfrac{1-n}{n\mathbf{B}(\mathbf{u}):\mathbf{D}(\mathbf{u})}\mathbf{B}(\mathbf{u})\otimes\mathbf{D}(\mathbf{u})\right),\\
\tilde{\boldsymbol{\varsigma}}(\mathbf{v}) &= 2H\tilde{\boldsymbol{\eta}}(\mathbf{u}) \star \mathbf{B}(\mathbf{v}),
\end{aligned} \tag{3.16}$$

cf. $\tilde{\boldsymbol{\eta}}$ and $\tilde{\boldsymbol{\sigma}}$ of FS in (3.3). The adjoint equation derived in [16] is the stress equation in (3.15) with a constant H, $\mathbf{F}_\omega = 0$ and $\tilde{\boldsymbol{\eta}}(\mathbf{u}) = \eta(\mathbf{u})$.

The adjoint SSA equations have the same structure as the adjoint FS equations (3.2). There is one stress equation for the adjoint velocity $\mathbf{v}$ and one equation for the multiplier ψ corresponding to the height equation in (2.10). However, the advection equation in (3.15) depends on the adjoint velocity $\mathbf{v}$ which leads to a fully coupled system for $\mathbf{v}$ and ψ.

The equations are solved backward in time with a final condition on ψ at $t = T$. As in (2.10), there is no time derivative in the stress equation. With a Weertman friction law, $f(\mathbf{u}) = \|\mathbf{u}\|^{m-1}$ and $f_\gamma(\mathbf{t}\cdot\mathbf{u}) = |\mathbf{t}\cdot\mathbf{u}|^{m-1}$, it is shown in Appendix A.1 that

$$\mathbf{F}_\omega(\mathbf{u}) = \frac{m-1}{\mathbf{u}\cdot\mathbf{u}}\mathbf{u}\otimes\mathbf{u}, \quad F_\gamma = m - 1.$$

If the friction coefficient C at the ice base is changed by δC, the bottom topography is changed by δb, and the lateral friction coefficient C_γ is changed by δC_γ, then it follows from Appendix A.2 that the Lagrangian is changed by

(3.17)
$$\begin{aligned}
\delta\mathcal{L} = &\int_0^T\int_\omega (2\eta\mathbf{B}(\mathbf{u}) : \mathbf{D}(\mathbf{v}) + \rho g\mathbf{v}\cdot\nabla h + \nabla\psi\cdot\mathbf{u})\,\delta b - f(\mathbf{u})\mathbf{u}\cdot\mathbf{v}\,\delta C\,\mathrm{d}\mathbf{x}\,\mathrm{d}t\\
&- \int_0^T\int_{\gamma_g} f_\gamma(\mathbf{t}\cdot\mathbf{u})\mathbf{t}\cdot\mathbf{u}\,\mathbf{t}\cdot\mathbf{v}\,\delta C_\gamma\,\mathrm{d}s\,\mathrm{d}t.
\end{aligned}$$

The weight in front of δC in (3.17) is actually the same as in (3.6).

Suppose that h is observed with $F_{\mathbf{u}} = 0$ in (3.15). Then the adjoint height equation must be solved for $\psi \neq 0$ to have a $\mathbf{v} \neq \mathbf{0}$ in the adjoint stress equation and a

perturbation in the Lagrangian in (3.17). The same conclusion followed from the adjoint FS equations.

The SSA model is obtained from the FS model in [6, 15] under some simplifying assumptions in the stress equation. An alternative derivation of the adjoint SSA would be to simplify the stress equation for $\mathbf{v}$ in the adjoint FS equations (3.2) under the same assumptions. The resulting adjoint equation would be different from (3.15) since the advection equation there depends on the adjoint velocity.

3.2.1. SSA in 2D. The forward and adjoint SSA equations in 2D are derived from (2.10) and (3.15) by letting H and u_1 be independent of y and taking $u_2 = 0$. There is no lateral force so that $C_\gamma = 0$. The position of the grounding line, where the ice starts floating on water, is denoted by x_{GL} as in Figure 1 and $\Gamma_b = [0, x_{GL}]$, $\Gamma_w = (x_{GL}, L]$. Let C be a positive constant on the bedrock and $C = 0$ on the water. Simplify the notation with $u = u_1$ and $v = v_1$. The forward equation is

$$\begin{aligned} &h_t + (uH)_x = a, \ \ 0 \le t \le T, \ 0 \le x \le L, \\ &h(x,0) = h_0(x), \ h(0,t) = h_L(t), \\ &(H\eta u_x)_x - Cf(u)u - \rho g H h_x = 0, \\ &u(0,t) = u_l(t), \ u(L,t) = u_c(t), \end{aligned} \tag{3.18}$$

where u_l is the speed of the flux of ice at $x = 0$ and u_c is the so-called calving rate at $x = L$. By the stress balance in (2.11), the calving front boundary satisfies

$$u_x(L,t) = A\left[\frac{\rho g H(L,t)}{4}(1 - \frac{\rho}{\rho_w})\right]^n.$$

Assume that $u > 0$ and $u_x > 0$, then $\eta = 2A^{-\frac{1}{n}} u_x^{\frac{1-n}{n}}$ and the friction term with a Weertman law is $Cf(u)u = Cu^m$. The adjoint equations for v and ψ follow either from simplifying the adjoint equations (3.15) or deriving the adjoint equations from the 2D forward SSA (3.18)

$$\begin{aligned} &\psi_t + u\psi_x + (\eta u_x - \rho g H)v_x + \rho g b_x v = F_h, \quad 0 \le t \le T, \ 0 \le x \le L, \\ &\psi(x,T) = 0, \ \psi(L,t) = 0, \\ &(\tfrac{1}{n}\eta H v_x)_x - Cmf(u)v - H\psi_x = -F_u, \\ &v(0,t) = 0, \ v(L,t) = 0. \end{aligned} \tag{3.19}$$

The coefficient $1/n$ in front of η in the equation for v is a result of the adjoint viscosity $\tilde{\boldsymbol{\eta}}$, which was 1 in the inexact adjoint SSA formulation in [16].

The effect on the Lagrangian of perturbations δb and δC is obtained from (3.17)

$$\delta\mathcal{L} = \int_0^T \int_0^L (\psi_x u + v_x \eta u_x + v\rho g h_x)\,\delta b - v f(u) u\,\delta C \ \mathrm{d}x\,\mathrm{d}t. \tag{3.20}$$

The results are almost identical with the SSA model when the friction coefficient is perturbed temporally as in Figure 2 with the FS model.

3.2.2. The forward steady state solution. The viscosity terms in (3.18) and (3.19) are often small and the longitudinal stress can be ignored in the steady state solution, see e.g. [27]. The approximations of both the forward and adjoint equations

can then be solved analytically on a reduced computational domain with $x \in [0, x_{GL}]$. The simplified forward steady state equation in (3.18) with $f(u) = u^{m-1}$ is written as

$$\begin{aligned} &(uH)_x = a,\ 0 \le x \le x_{GL}, \\ &H(0) = H_0, \\ &-Cu^m - \rho g H h_x = 0, \\ &u(0) = 0, \end{aligned} \tag{3.21}$$

and the adjoint equation in (3.19) is simplified when b_x is small

$$\begin{aligned} &u\psi_x - \rho g H v_x = F_h,\ \ 0 \le x \le x_{GL}, \\ &\psi_x(0) = 0,\ \psi(x_{GL}) = 0, \\ &-Cmu^{m-1}v - H\psi_x = -F_u, \\ &v(0) = 0. \end{aligned} \tag{3.22}$$

Numerical experiments show that a more accurate solution compared to the FS solution is obtained by calibration of H with $H_{GL} = H(x_{GL})$ in (3.21). All the assumptions made for the simplification in (3.21) are not valid close to the ice divide at $x = 0$ and the ice dynamics in this area cannot be captured accurately by SSA.

The solution to the forward equation (3.21) is determined when a and C are constant in (B.3) and (B.4) in Appendix B by integrating (B.2) from x to x_{GL}

$$\begin{aligned} H(x) &= \left(H_{GL}^{m+2} + \frac{m+2}{m+1}\frac{Ca^m}{\rho g}(x_{GL}^{m+1} - x^{m+1}) \right)^{\frac{1}{m+2}},\ 0 \le x \le x_{GL}, \\ H(x) &= H_{GL},\ x_{GL} < x < L, \\ u(x) &= \frac{ax}{H},\ 0 \le x \le x_{GL}, \quad u(x) = \frac{ax}{H_{GL}},\ x_{GL} < x < L. \end{aligned} \tag{3.23}$$

An example of the analytical solutions $u(x)$ and $H(x)$ for $x \in [0, x_{GL}]$ is given in Figure 3. When x approaches x_{GL}, then u increases and H decreases rapidly. The details of this example are found in [2]. An alternative solution to (3.18) when $x > x_{GL}$ is found in [6] where the assumption is that $H(x)$ is linear in x.

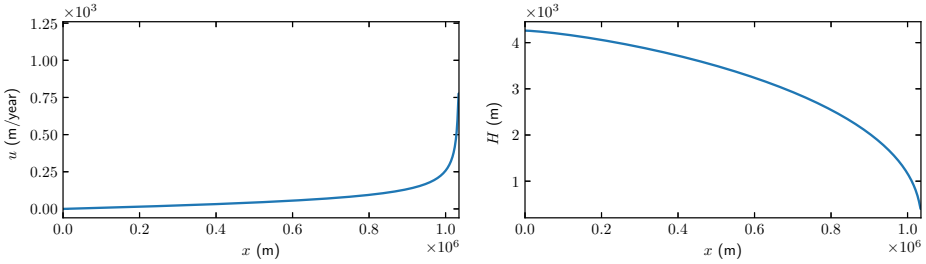

FIG. 3. *The analytical solutions $u(x)$ and $H(x)$ in (3.23) for a grounded ice in $[0, x_{GL}]$.*

3.2.3. The adjoint steady state solution with $F_u \neq 0$. The analytical solutions to (3.21) and (3.22) are derived in Appendix B to Appendix D by assuming b_x small, $b_x \ll H_x$, and a and C constant. The expressions for ψ and v are found in (D.1)-(D.4). A variable with the subscript $*$ is evaluated at x_*. When u is observed at x_*, then $\mathcal{F}$ and $F(u, h)$ are

$$\mathcal{F} = \int_0^L u(x)\delta(x - x_*)\,\mathrm{d}x = u_*,\ F_u = \delta(x - x_*),\ F_h = 0,$$

and the adjoint solutions are

$$
\begin{aligned}
\psi(x) &= \frac{Ca^m x_*}{\rho g H_*^{m+3}} \left(x_{GL}^m - x^m\right),\ x_* < x \le x_{GL},\\
\psi(x) &= -\frac{1}{H_*} + \frac{Ca^m x_*}{\rho g H_*^{m+3}} \left(x_{GL}^m - x_*^m\right),\ 0 \le x < x_*,\\
v(x) &= \frac{ax_*}{\rho g H_*^{m+3}} H^m,\ x_* < x \le x_{GL},\\
v(x) &= 0,\ 0 \le x < x_*,
\end{aligned}
\tag{3.24}
$$

with discontinuities at the observation point x_* in $\psi(x)$ and $v(x)$. The analytical solutions $\psi(x)$ and $v(x)$ of the ice sheet in Figure 3 at different x_* positions are shown in the left panels of Figure 4 and Figure 5. In all figures, $m = 1$.

The perturbation of the Lagrangian in (3.20) is derived in (D.5)-(D.6) in Appendix D

$$
\begin{aligned}
\frac{\delta u_*}{u_*} &= u_*^{-1}\delta\mathcal{L} = u_*^{-1}\int_0^{x_{GL}} \left(\psi_x u + v_x \eta u_x + v\rho g h_x\right)\delta b - v u^m\,\delta C\ \mathrm{d}x\\
&= \int_{x_*^-}^{x_{GL}} \frac{H^m}{H_*^{m+2}}\left[(m+1)H_x\mathcal{H}(x-x_*) + H\delta(x-x_*)\right]\delta b - \frac{(ax)^m}{\rho g H_*^{m+2}}\,\delta C\ \mathrm{d}x\\
&= \frac{\delta b_*}{H_*} - \frac{1}{\rho g H_*^{m+2}}\int_{x_*}^{x_{GL}} C(ax)^m\left((m+1)\frac{\delta b}{H} + \frac{\delta C}{C}\right)\ \mathrm{d}x,
\end{aligned}
\tag{3.25}
$$

and the weights with respect to δC and δb are shown in the left panels of Figure 6 and Figure 7 for the same ice sheet geometry as in Figure 3. The weight in front of δC increases when $x_* \to x_{GL}$. This is an effect of the increasing velocity u_* and the decreasing thickness H_*, see Figure 3. A perturbation δC with support in $[x_*, x_{GL}]$ will cause larger perturbations at the surface the closer x_* is to x_{GL} and the closer $\delta C(x)$ is to x_{GL}. The change in u_* due to δb in (3.25) is simplified based on the assumption $H_x \ll H$ such that $\delta u_* = u_*\delta b_*/H_*$. Consequently, the main effect on u_* from the perturbation δb is localized at each x_*. In Figure 7, the weight functions of δb are shown in the same range as the weights of δC in Figure 6, although the coefficient multiplying the Dirac delta term in (D.6) is several magnitudes larger ($\sim 10^9$ in this case) which exceeds the ordinate limit of this figure.

Perturb C by $\delta C = \epsilon\cos(kx/x_{GL})$ in (3.25) for some wave number k and let $\delta b = 0$ and $m = 1$. Then

$$
\begin{aligned}
\delta u_* &= -\int_{x_*}^{x_{GL}} \epsilon\frac{a^2 x_*}{\rho g H_*^4} x\cos\left(\frac{kx}{x_{GL}}\right)\ \mathrm{d}x\\
&= -\epsilon\frac{a^2 x_*}{\rho g H_*^4}\frac{x_{GL}}{k}\left(x_{GL}\sin(k) - x_*\sin\left(\frac{kx_*}{x_{GL}}\right) + \frac{x_{GL}}{k}\left(\cos(k) - \cos\left(\frac{kx_*}{x_{GL}}\right)\right)\right).
\end{aligned}
\tag{3.26}
$$

When k grows at the ice base, the amplitude of the perturbation at the ice surface decays as $1/k$. The effect of high wave number perturbations of C will be difficult to observe at the top of the ice. This is in contrast to the SIA model in (3.36) where all perturbations at the base, regardless of the wave number, will be propagated undamped to the surface.

Let the friction coefficient C be perturbed by a constant δC in $[0, x_{GL}]$ and take $\delta b = 0$. Then it follows from (3.25) that

$$
\delta u_* = \delta C\int_{x_*}^{x_{GL}} -v u^m\,\mathrm{d}x = \frac{a^{m+1}x_*(x_*^{m+1} - x_{GL}^{m+1})}{(m+1)\rho g H_*^{m+3}}\,\delta C
\tag{3.27}
$$

Computing the derivative of $u(x, C)$ with respect to C in the explicit expression in (3.23) at x_* yields the same result.

The sensitivity of surface data to changes in b and C is estimated in [9] with a linearized model. The conclusion is that differences of short wavelength in the bedrock topography can be observed at the surface but only differences with long wavelength in the friction coefficient propagate to the top of the ice. This is in agreement with (3.25) and (3.26).

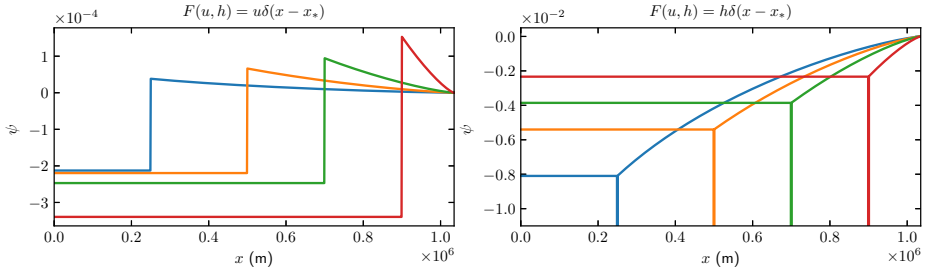

FIG. 4. *The analytical solutions of ψ in (3.22) of the observations of u (left panel) and h (right panel) at different locations $x_* = 0.25 \times 10^6, 0.5 \times 10^6, 0.7 \times 10^6$ and 0.9×10^6 m (blue, orange, green and red). The expression of ψ with respect to the observation of u is in (3.24) and the h response is in (3.28).*

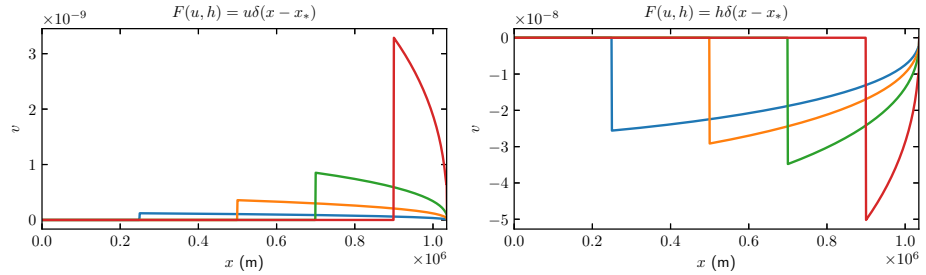

FIG. 5. *The analytical solutions of v in (3.22) of the observations of u (left panel) and h (right panel) at different locations $x_* = 0.25 \times 10^6, 0.5 \times 10^6, 0.7 \times 10^6$ and 0.9×10^6 m (blue, orange, green and red). The expression of v with respect to the observation of u is in (3.24) and the continuous part of the h response is in (3.28).*

3.2.4. The adjoint steady state solution with $F_h \neq 0$. In the case when h is observed at x_* and $F_u = 0$ and $F_h = \delta(x - x_*)$, the expressions for ψ and v are

$$
\begin{aligned}
\psi(x) &= -\frac{Ca^{m-1}}{\rho g H_*^{m+1}} \left(x_{GL}^m - x^m\right), \ x_* < x \leq x_{GL}, \\
\psi(x) &= -\frac{Ca^{m-1}}{\rho g H_*^{m+1}} \left(x_{GL}^m - x_*^m\right), \ 0 \leq x < x_*, \\
v(x) &= -\frac{H^m}{\rho g H_*^{m+1}}, \ x_* < x \leq x_{GL}, \\
v(x) &= 0, \ 0 \leq x < x_*.
\end{aligned}
\tag{3.28}
$$

There is a discontinuity at the observation point x_* in $v(x)$, see Figure 5, but $\psi(x)$ is continuous in the solution of (3.22). Actually, $\psi(x) \sim -\delta(x - x_*)$ in the neighborhood

of x_* due to the second derivative term $(\frac{1}{n}\eta H v_x)_x$ which is neglected in the simplified equation (3.22) but is of importance at x_*. A correction $\hat{\psi}$ of ψ at x_* is therefore introduced to satisfy $\left(\frac{1}{n}\eta H v_x\right)_x - H\hat{\psi}_x = 0$. With $v_x(x_*) = -\delta(x-x_*)/(\rho g H_*)$, the correction is $\hat{\psi}(x) = -\delta(x-x_*)\eta_*/(n\rho g H_*)$. The solution ψ is corrected at each x_* in Figure 4 with $\hat{\psi}$ which is a Dirac delta with a multiplying coefficient approximately 1000 times larger than ψ. The perturbation in h is as in (3.25) with ψ and v in (3.28) and the additional term $\hat{\psi}$

(3.29)
$$\begin{aligned}\frac{\delta h_*}{H_*} &= \int_{x_*^-}^{x_{GL}} -\frac{u\eta_*}{n\rho g H_*^2}\delta_x(x-x_*)\delta b\,\mathrm{d}x + \int_{x_*}^{x_{GL}} \frac{C(ax)^m}{\rho g H_*^{m+2}}\left((m+1)\frac{\delta b}{H}+\frac{\delta C}{C}\right)\,\mathrm{d}x\\ &= \frac{\eta_*}{n\rho g H_*^2}(u\delta b)_x(x_*) + \frac{1}{\rho g H_*^{m+2}}\int_{x_*}^{x_{GL}} C(ax)^m\left((m+1)\frac{\delta b}{H}+\frac{\delta C}{C}\right)\,\mathrm{d}x,\end{aligned}$$

where $(u\delta b)_x(x_*)$ represents the x-derivative of $u\delta b$ evaluated at x_*. When $\delta b = 0$ then δu_* in (3.25) and $\delta h_* = \delta H_*$ in (3.29) satisfy $\delta u_* H_* = -\delta H_* u_*$ as in the integrated form of the advection equation in (3.21) and in (B.1). The contribution from the integrals in (3.25) and (3.29) is identical except for the sign.

The adjoint variable v and the weights for δC in the right panels where $F_h \neq 0$ of Figures 5 and 6 behave in the same manner as in the left panels where $F_u \neq 0$ but with a change of sign.

In Figure 7, as $u\psi_x$ dominates the weights for δb in (3.29), $\hat{\psi}$ contributes with a term proportional to $-\delta_x(x-x_*)$ at x_* whose coefficient is several magnitudes ($\sim 10^8$ in this case) larger than the remaining weight function. Therefore, the main perturbation in h is due to the x-derivative of $u\delta b$ at x_*. If $u\delta b$ is constant, then δh is determined by the continuous weight in $x \in [x_*, x_{GL}]$ which has a shape similar to the δC weight in Figure 6. A perturbation of b at the base is directly visible locally in u at the surface while the effect of δC is non-local in (3.25).

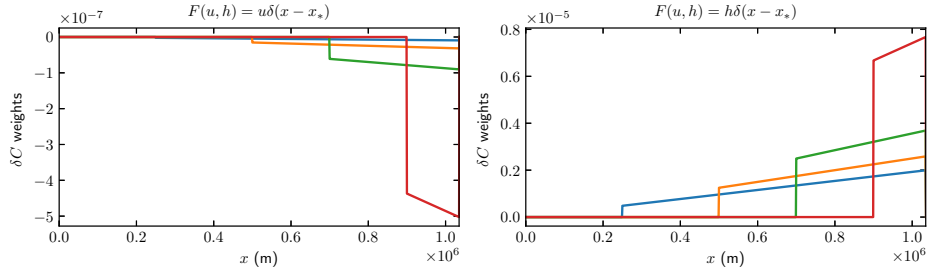

FIG. 6. *The analytical solution of the weights $-vu^m$ on δC in (3.20) for the observations of u (left panel) and h (right panel) at different locations $x_* = 0.25\times 10^6, 0.5\times 10^6, 0.7\times 10^6$ and 0.9×10^6 m (blue, orange, green and red). The expressions are given in (D.5).*

3.3. Shallow ice approximation. With $C_b = 0$ and no sliding at the ice base, it follows from (2.12) that

(3.30)
$$\begin{aligned}\mathbf{Q}(x,y,t) &= -\frac{2}{n+2}A(\rho g)^n\|\nabla h\|^{n-1}\nabla h H^{n+2}\\ &= \frac{n+1}{n+2}\mathbf{u}(x,y,h,t)H(x,y,t),\end{aligned}$$

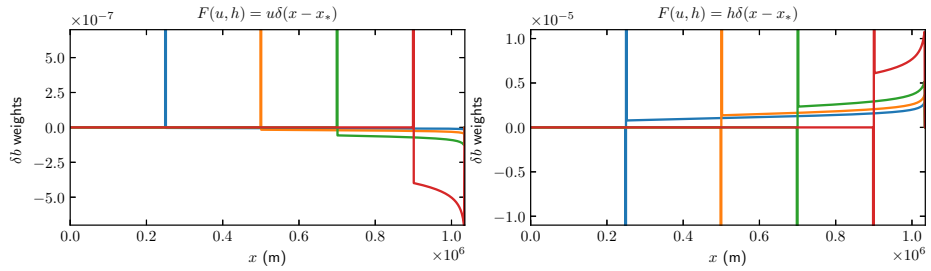

FIG. 7. *The analytical solution of the weights* $\psi_x u + v_x \eta u_x + v\rho g h_x$ *on* δb *in* (3.20) *for the observations of* u *(left panel) and* h *(right panel) at different locations* $x_* = 0.25\times10^6, 0.5\times10^6, 0.7\times10^6$ *and* 0.9×10^6 *m (blue, orange, green and red). The expressions are given in* (D.6).

and at the steady state in (2.13) the flux satisfies

$$\nabla \cdot \mathbf{Q} = a \tag{3.31}$$

In this case, there is no need to solve an adjoint equation to estimate the perturbation when C_b is increased by $\delta C_b > 0$.

Consider the steady state solution of (3.31) in 2D with the unknown $u_1(x,h)$ and $H(x)$ in $[x_L, x_R]$. By (3.30) and (3.31) with $C_b = 0$

$$Q_x = \frac{n+1}{n+2}(u_1 H)_x = a(x),\ x \in [x_L, x_R]. \tag{3.32}$$

The solution of (3.32) is

$$u_1 H(x) = u_1 H(x_L) + \alpha(x),\ \alpha(x) = \frac{n+2}{n+1}\int_{x_L}^{x} a(\xi)\,\mathrm{d}\xi. \tag{3.33}$$

After division by $u_1(x,h)$

$$H(x) = \frac{u_1 H(x_L) + \alpha(x)}{u_1(x,h)} = -\frac{n+1}{2}\frac{u_1 H(x_L) + \alpha(x)}{A(\rho g)^n |h_x|^{n-1} h_x H^{n+1}}$$

and solving for $H(x)$ we obtain

$$H(x) = \left(-\frac{n+1}{2}\frac{u_1 H(x_L) + \alpha(x)}{A(\rho g)^n |h_x|^{n-1} h_x}\right)^{\frac{1}{n+2}}. \tag{3.34}$$

Perturbations δu_1 and δH in u_1 and H at the steady state in (3.33) satisfy

$$H\delta u_1 + u_1 \delta H = 0. \tag{3.35}$$

Introduce sliding at $z = b$ with $\delta C_b > 0$. Then directly by (2.12), (3.35), and the definition of H

$$\begin{aligned} \delta u_1 &= -(\rho g H)^{\theta-\lambda} |h_x|^{\theta-1} h_x \delta C_b, \\ \delta H &= -\frac{H}{u_1}\delta u_1 = -\frac{n+1}{2A}(\rho g H)^{\theta-\lambda-n} |h_x|^{\theta-n}\, \delta C_b. \end{aligned} \tag{3.36}$$

A perturbation in C_b at x will perturb u_1 and H at the ice surface only at x in the SIA model.

4. Conclusions. The sensitivity of the flow of ice on basal conditions is analyzed for time dependent and steady state solutions of the FS, SIA, and SSA equations including the advection equation for the height. Perturbations at the base of the ice are introduced in the friction coefficient C and the topography b. The analysis is based on the adjoint equations of the FS and SSA stress and advection equations. The adjoint FS and SSA equations follow from the Lagrangians of the forward FS and SSA equations.

The adjoint equations are derived for observations of the velocity $\mathbf{u}$ and height h on the top surface of the ice. The adjoint height equation in the FS model is solved analytically in 2D. The relation between the inverse problem to find parameters from data and the sensitivity problem is established. If the perturbations in the basal conditions are time dependent then time cannot be ignored in the inversion. The wrong conclusions may be drawn with only static snapshots of $\mathbf{u}$ and h. It is necessary to include the adjoint height equation if h is observed.

The adjoint equations of the FS and SSA models are similar and the analytical solutions based on the SSA equations in 2D show that the sensitivity grows as the observation point x_* is approaching the grounding line separating the grounded and the floating parts of the ice. The reason is that the velocity increases and the thickness of the ice decreases.

In SSA, there is a non-local effect of a perturbation δC in C in the sense that $\delta C(x)$ affects both $u(x_*)$ and $h(x_*)$ even if $x \neq x_*$, but δb has a strong local effect concentrated at x_*. Nevertheless, the shapes of the two sensitivity functions for δb and dC are very similar except for the neighborhood of x_*. It is possible to separate the effect of δb and δC in the steady state SSA model thanks to the localized influence of δb in δu and δh in (3.25) and (3.29). In the steady state SSA solution, an increase of the friction coefficient C at x_* leads to a decrease in u but an increase in h in the domain downstream of x_*. On the other hand, an increase of the bedrock elevation b at x_* causes an increase in u at the same position, but in the downstream direction, it reduces the velocity u. Perturbations in C at the base observed in u at the surface are damped inversely proportional to the wavenumber of δC thus making high frequency perturbations difficult to register at the top. The sensitivity in u in the SIA model is local to basal perturbations in the sliding coefficient.

The numerical results in [2] confirm the conclusions here and are in good agreement with the analytical solutions.

Appendix A. Derivation of the adjoint equations.

A.1. Adjoint viscosity and friction in SSA. The adjoint viscosity $\tilde{\boldsymbol{\eta}}(\mathbf{u})$ in SSA in (3.3) is derived as follows. The SSA viscosity for $\mathbf{u}$ and $\mathbf{u}+\delta\mathbf{u}$ is

(A.1)
$$\eta(\mathbf{u}+\delta\mathbf{u}) \approx \eta(\mathbf{u})\left(1+\frac{1-n}{2n}\frac{(2u_{1x}+u_{2y})\delta u_{1x}+\frac{1}{2}(u_{1y}+u_{2x})\delta u_{2x}+(2u_{2y}+u_{1x})\delta u_{2y}+\frac{1}{2}(u_{1y}+u_{2x})\delta u_{1y}}{\hat{\eta}}\right).$$

Determine $\mathcal{B}(\mathbf{u})$ such that

$$\varrho(\mathbf{u},\delta\mathbf{u})\mathbf{B}(\mathbf{u}) = \mathcal{B}(\mathbf{u})\star\mathbf{B}(\delta\mathbf{u}).$$

First note that

$$\begin{aligned}&\mathbf{B}(\mathbf{u}):\mathbf{D}(\delta\mathbf{u}) = (\mathbf{D}(\mathbf{u}) + \nabla\cdot\mathbf{u}\mathbf{I}):\mathbf{D}(\delta\mathbf{u}) = \mathbf{D}(\mathbf{u}):\mathbf{D}(\delta\mathbf{u}) + (\nabla\cdot\mathbf{u})(\nabla\cdot\delta\mathbf{u})\\ &= \mathbf{D}(\mathbf{u}):(\mathbf{B}(\delta\mathbf{u}) - \nabla\cdot\delta\mathbf{u}\mathbf{I}) + (\nabla\cdot\mathbf{u})(\nabla\cdot\delta\mathbf{u}) = \mathbf{D}(\mathbf{u}):\mathbf{B}(\delta\mathbf{u}).\end{aligned}$$

Then use the $\star$ operator in (3.5) to define $\mathcal{B}$

$$\begin{aligned}\tfrac{1-n}{2n\hat{\eta}}\textstyle\sum_{kl} B_{kl}(\mathbf{u})D_{kl}(\delta\mathbf{u})B_{ij}(\mathbf{u}) &= \tfrac{1-n}{2n\hat{\eta}}\textstyle\sum_{kl} D_{kl}(\mathbf{u})B_{kl}(\delta\mathbf{u})B_{ij}(\mathbf{u})\\ &= \textstyle\sum_{kl}\mathcal{B}_{ijkl}(\mathbf{u})D_{kl}(\delta\mathbf{u}) = (\mathcal{B}\star D)_{ij}.\end{aligned}$$

Thus, let

$$\mathcal{B}_{ijkl} = \frac{1-n}{2n\hat{\eta}}B_{ij}(\mathbf{u})D_{kl}(\mathbf{u}),\quad \tilde{\eta}_{ijkl}(\mathbf{u}) = \eta(\mathbf{u})(\mathcal{I}_{ijkl} + \mathcal{B}_{ijkl}(\mathbf{u})),$$

or in tensor form

$$\mathcal{B} = \frac{1-n}{n\mathbf{B}(\mathbf{u}):\mathbf{D}(\mathbf{u})}\mathbf{B}(\mathbf{u})\otimes\mathbf{D}(\mathbf{u}),\quad \tilde{\boldsymbol{\eta}}(\mathbf{u}) = \eta(\mathbf{u})\left(\mathcal{I} + \mathcal{B}\right). \tag{A.2}$$

Replacing $\mathbf{B}$ in (A.2) by $\mathbf{D}$ we obtain the adjoint FS viscosity in (3.3).

The adjoint friction in SSA in ω and at γ_g in (3.15) with a Weertman law is derived as in the adjoint FS equations (3.2) and (3.3). Then in ω with $\boldsymbol{\xi} = \mathbf{u}, \boldsymbol{\zeta} = \mathbf{v}, c = C, \mathbf{F} = \mathbf{F}_b$, and at γ_g with $\boldsymbol{\xi} = \mathbf{t}\cdot\mathbf{u}, \boldsymbol{\zeta} = \mathbf{t}\cdot\mathbf{v}, c = C_\gamma, f = f_\gamma, \mathbf{F} = F_\gamma$, we arrive at

$$cf(\boldsymbol{\xi})\left(\mathbf{I} + \mathbf{F}(\boldsymbol{\xi})\right)\boldsymbol{\zeta},\quad \mathbf{F}(\boldsymbol{\xi}) = \frac{m-1}{\boldsymbol{\xi}\cdot\boldsymbol{\xi}}\boldsymbol{\xi}\otimes\boldsymbol{\xi}. \tag{A.3}$$

A.2. Adjoint equations in SSA. The Lagrangian for the SSA equations is with the adjoint variables $\psi, \mathbf{v}, q$

$$\begin{aligned}&\mathcal{L}(\mathbf{u}, h; \mathbf{v}, \psi; b, C_\gamma, C) = \textstyle\int_0^T\int_\omega F(\mathbf{u}, h) + \psi(h_t + \nabla\cdot(\mathbf{u}H) - a)\,\mathrm{d}\mathbf{x}\,\mathrm{d}t\\ &+ \textstyle\int_0^T\int_\omega \mathbf{v}\cdot\nabla\cdot(2H\eta\mathbf{B}(\mathbf{u})) - Cf(\mathbf{u})\mathbf{v}\cdot\mathbf{u} - \rho gH\mathbf{v}\cdot\nabla h\,\mathrm{d}\mathbf{x}\,\mathrm{d}t\\ &= \textstyle\int_0^T\int_\omega F(\mathbf{u}, h) + \psi(h_t + \nabla\cdot(\mathbf{u}H) - a)\,\mathrm{d}\mathbf{x}\,\mathrm{d}t\\ &+ \textstyle\int_0^T\int_\omega -2H\eta(\mathbf{u})(\mathbf{D}(\mathbf{v}):\mathbf{D}(\mathbf{u}) + \nabla\cdot\mathbf{u}\nabla\cdot\mathbf{v})\\ &-Cf(\mathbf{u})\mathbf{v}\cdot\mathbf{u} - \rho gH\mathbf{v}\cdot\nabla h\,\mathrm{d}\mathbf{x}\,\mathrm{d}t - \textstyle\int_0^T\int_{\gamma_g} C_\gamma f_\gamma(\mathbf{t}\cdot\mathbf{u})\mathbf{t}\cdot\mathbf{u}\,\mathbf{t}\cdot\mathbf{v}\,\mathrm{d}s\,\mathrm{d}t\end{aligned} \tag{A.4}$$

after partial integration and using the boundary conditions. The perturbed SSA Lagrangian is split into the unperturbed Lagrangian and three integrals

$$\begin{aligned}&\mathcal{L}(\mathbf{u}+\delta\mathbf{u}, h+\delta h; \mathbf{v}+\delta\mathbf{v}, \psi+\delta\psi; b+\delta b, C_\gamma+\delta C_\gamma, C+\delta C)\\ &= \textstyle\int_0^T\int_\omega F(\mathbf{u}+\delta\mathbf{u}, h+\delta h)\\ &+ \textstyle\int_0^T\int_\omega(\psi+\delta\psi)(h_t + \delta h_t + \nabla\cdot((\mathbf{u}+\delta\mathbf{u})(H+\delta H)) - a)\,\mathrm{d}\mathbf{x}\,\mathrm{d}t\\ &+ \textstyle\int_0^T\int_\omega -2(H+\delta H)\eta(\mathbf{u}+\delta\mathbf{u})\mathbf{D}(\mathbf{v}+\delta\mathbf{v}):\mathbf{B}(\mathbf{u}+\delta\mathbf{u})\\ &-(C+\delta C)f(\mathbf{u}+\delta\mathbf{u})(\mathbf{u}+\delta\mathbf{u})\cdot(\mathbf{v}+\delta\mathbf{v})\\ &-\rho g(H+\delta H)\nabla(h+\delta h)\cdot(\mathbf{v}+\delta\mathbf{v})\,\mathrm{d}\mathbf{x}\,\mathrm{d}t\\ &- \textstyle\int_0^T\int_{\gamma_g}(C_\gamma+\delta C_\gamma)f_\gamma(\mathbf{t}\cdot(\mathbf{u}+\delta\mathbf{u}))\mathbf{t}\cdot(\mathbf{u}+\delta\mathbf{u})\,\mathbf{t}\cdot(\mathbf{v}+\delta\mathbf{v})\,\mathrm{d}s\,\mathrm{d}t\\ &= \mathcal{L}(\mathbf{u}, h; \mathbf{v}, \psi; b, C_\gamma, C) + I_1 + I_2 + I_3.\end{aligned} \tag{A.5}$$

The perturbation in $\mathcal{L}$ is

$$\delta\mathcal{L} = I_1 + I_2 + I_3. \tag{A.6}$$

Terms of order two or more in $\delta\mathcal{L}$ are neglected. Then the first term in $\delta\mathcal{L}$ satisfies

$$\begin{aligned} I_1 &= \int_0^T \int_\omega F(\mathbf{u}+\delta\mathbf{u}, h+\delta h) - F(\mathbf{u}, h)\,\mathrm{d}\mathbf{x}\,\mathrm{d}t \\ &= \int_0^T \int_\omega F_{\mathbf{u}}\delta\mathbf{u} + F_h\delta h\,\mathrm{d}\mathbf{x}\,\mathrm{d}t. \end{aligned} \tag{A.7}$$

Using partial integration, Gauss' formula, and the initial and boundary conditions on $\mathbf{u}$ and H and $\psi(\mathbf{x}, T) = 0, \mathbf{x} \in \omega$, and $\psi(\mathbf{x}, t) = 0,\ \mathbf{x} \in \gamma_w$, in the second integral we have

$$\begin{aligned} I_2 &= \int_0^T \int_\omega \delta\psi(h_t + \nabla\cdot(\mathbf{u}H) - a) \\ &\quad +\psi(\delta h_t + \nabla\cdot(\delta\mathbf{u}H) + \nabla\cdot(\mathbf{u}\delta H))\,\mathrm{d}\mathbf{x}\,\mathrm{d}t \\ &= \int_0^T \int_\omega \delta\psi(h_t + \nabla\cdot(\mathbf{u}H) - a)\,\mathrm{d}\mathbf{x}\,\mathrm{d}t \\ &\quad + \int_0^T \int_\omega -\psi_t\delta h - H\nabla\psi\cdot\delta\mathbf{u} - \nabla\psi\cdot\mathbf{u}\delta H\,\mathrm{d}\mathbf{x}\,\mathrm{d}t. \end{aligned} \tag{A.8}$$

The first integral after the second equality vanishes since h is a weak solution and I_2 is

$$I_2 = \int_0^T \int_\omega -(\psi_t + \mathbf{u}\cdot\nabla\psi)\delta h - H\nabla\psi\cdot\delta\mathbf{u} + \mathbf{u}\cdot\nabla\psi\delta b\,\mathrm{d}\mathbf{x}\,\mathrm{d}t. \tag{A.9}$$

Using the weak solution of (2.10), the adjoint viscosity (3.16), (A.2), the friction coefficient (A.3), Gauss' formula, the boundary conditions, and neglecting the second order terms, the third and fourth integrals in (A.5) are

$$\begin{aligned} I_3 &= I_{31} + I_{32}, \\ I_{31} &= \int_0^T \int_\omega -2(H+\delta H)\eta(\mathbf{u}+\delta\mathbf{u})\mathbf{D}(\mathbf{v}+\delta\mathbf{v}) : \mathbf{B}(\mathbf{u}+\delta\mathbf{u}) \\ &\quad -(C+\delta C)f(\mathbf{u}+\delta\mathbf{u})(\mathbf{u}+\delta\mathbf{u})\cdot(\mathbf{v}+\delta\mathbf{v}) \\ &\quad -\rho g(H+\delta H)\nabla(h+\delta h)\cdot(\mathbf{v}+\delta\mathbf{v}))\,\mathrm{d}\mathbf{x}\,\mathrm{d}t \\ &\quad -\int_0^T \int_\gamma (C_\gamma + \delta C_\gamma) f_\gamma(\mathbf{t}\cdot(\mathbf{u}+\delta\mathbf{u}))\mathbf{t}\cdot(\mathbf{u}+\delta\mathbf{u})\,\mathbf{t}\cdot(\mathbf{v}+\delta\mathbf{v})\,\mathrm{d}s\,\mathrm{d}t \\ &= I_{311} + I_{312} - I_{313}, \end{aligned} \tag{A.10}$$

where

$$\begin{aligned} I_{311} &= \int_0^T \int_\omega -2H\mathbf{D}(\mathbf{v}) : (\eta(\mathbf{u}+\delta\mathbf{u})\mathbf{B}(\mathbf{u}+\delta\mathbf{u})) \\ &\quad +2H\mathbf{D}(\mathbf{v}) : (\eta(\mathbf{u})\mathbf{B}(\mathbf{u}))\,\mathrm{d}\mathbf{x}\,\mathrm{d}t \\ &= \int_0^T \int_\omega -2H\mathbf{D}(\mathbf{v}) : (\tilde{\boldsymbol{\eta}}(\mathbf{u}) \star \mathbf{B}(\delta\mathbf{u}))\,\mathrm{d}\mathbf{x}\,\mathrm{d}t \\ I_{312} &= \int_0^T \int_{\omega_g} -\delta C f(\mathbf{u})\mathbf{u}\cdot\mathbf{v}\,\mathrm{d}\mathbf{x}\,\mathrm{d}t \\ &\quad + \int_0^T \int_{\omega_g} -C(f(\mathbf{u}+\delta\mathbf{u})\mathbf{v}\cdot(\mathbf{u}+\delta\mathbf{u}) - f(\mathbf{u})\mathbf{v}\cdot\mathbf{u})\,\mathrm{d}\mathbf{x}\,\mathrm{d}t \\ &= \int_0^T \int_{\omega_g} -\delta C f(\mathbf{u})\mathbf{u}\cdot\mathbf{v} + Cf(\mathbf{u})(\mathbf{I} + \mathbf{F}_b(\mathbf{u}))\delta\mathbf{u}\cdot\mathbf{v}\,\mathrm{d}\mathbf{x}\,\mathrm{d}t \\ I_{313} &= \int_0^T \int_{\gamma_g} (C_\gamma + \delta C_\gamma)(f_\gamma(\mathbf{t}\cdot(\mathbf{u}+\delta\mathbf{u}))\mathbf{t}\cdot\mathbf{v}\,\mathbf{t}\cdot(\mathbf{u}+\delta\mathbf{u}) \\ &\quad -f_\gamma(\mathbf{t}\cdot\mathbf{u})\mathbf{t}\cdot\mathbf{v}\,\mathbf{t}\cdot\mathbf{u})\,\mathrm{d}s\,\mathrm{d}t \\ &= \int_0^T \int_{\gamma_g} (C_\gamma + \delta C_\gamma)(f_\gamma(\mathbf{t}\cdot\mathbf{u})\mathbf{t}\cdot\mathbf{u}\,\mathbf{t}\cdot\mathbf{v} \\ &\quad +C_\gamma f_\gamma(\mathbf{t}\cdot\mathbf{u})(\mathbf{I} + \mathbf{F}_\gamma(\mathbf{t}\cdot\mathbf{u}))\mathbf{t}\cdot\delta\mathbf{u}\,\mathbf{t}\cdot\mathbf{v}\,\mathrm{d}s\,\mathrm{d}t \\ I_{32} &= \int_0^T \int_\omega -\rho g H\nabla h\cdot\mathbf{v} - 2\eta\mathbf{D}(\mathbf{v}) : \mathbf{B}(\mathbf{u})\delta H \\ &\quad -\rho g\nabla h\cdot\mathbf{v}\delta H - \rho g H\mathbf{v}\cdot\nabla\delta h\,\mathrm{d}\mathbf{x}\,\mathrm{d}t \\ &= \int_0^T \int_\omega -\rho g H\nabla h\cdot\mathbf{v} - (2\eta\mathbf{D}(\mathbf{v}) : \mathbf{B}(\mathbf{u}) + \rho g\nabla h\cdot\mathbf{v})\delta H \\ &\quad +\rho g\nabla\cdot(H\mathbf{v})\delta h\,\mathrm{d}\mathbf{x}\,\mathrm{d}t. \end{aligned} \tag{A.11}$$

Collecting all the terms in (A.7), (A.9), and (A.10), the first variation of $\mathcal{L}$ is

$$
\begin{aligned}
\delta\mathcal{L} &= I_1 + I_2 + I_3 \\
&= \int_0^T \int_\omega F_{\mathbf{u}}\delta\mathbf{u} - 2HD(\mathbf{v}) : (\tilde{\boldsymbol{\eta}}(\mathbf{u}) \star \mathbf{B}(\delta\mathbf{u})) - H\nabla\psi\cdot\delta\mathbf{u}\,\mathrm{d}\mathbf{x}\,\mathrm{d}t \\
&\quad - \int_0^T \int_{\omega_g} Cf(\mathbf{u})(\mathbf{I}+\mathbf{F}_b(\mathbf{u}))\mathbf{v}\cdot\delta\mathbf{u}\,\mathrm{d}\mathbf{x}\,\mathrm{d}t \\
&\quad - \int_0^T \int_{\gamma_g} C_\gamma f_\gamma(\mathbf{t}\cdot\mathbf{u})(\mathbf{I}+\mathbf{F}_\gamma(\mathbf{t}\cdot\mathbf{u}))\mathbf{t}\cdot\mathbf{v}\,\mathbf{t}\cdot\delta\mathbf{u}\,\mathrm{d}s\,\mathrm{d}t \\
&\quad - \int_0^T \int_{\gamma_g} \delta C_\gamma f_\gamma(\mathbf{t}\cdot\mathbf{u})\mathbf{t}\cdot\mathbf{u}\,\mathbf{t}\cdot\mathbf{v}\,\mathrm{d}s\,\mathrm{d}t \\
&\quad + \int_0^T \int_\omega (F_h - (\psi_t + \mathbf{u}\cdot\nabla\psi + 2\eta\mathbf{D}(\mathbf{v}) : \mathbf{B}(\mathbf{u}) \\
&\quad - \rho g\nabla b\cdot\mathbf{v} + \rho g H\nabla\cdot\mathbf{v}))\delta h\,\mathrm{d}\mathbf{x}\,\mathrm{d}t \\
&\quad + \int_0^T \int_\omega -\delta C f(\mathbf{u})\mathbf{v}\cdot\mathbf{u} \\
&\quad + (2\eta\mathbf{D}(\mathbf{v}) : \mathbf{B}(\mathbf{u}) + \rho g\nabla h\cdot\mathbf{v} + \mathbf{u}\cdot\nabla\psi)\delta b\,\mathrm{d}\mathbf{x}\,\mathrm{d}t.
\end{aligned} \tag{A.12}
$$

The forward solution $(\mathbf{u}^*, p^*, h^*)$ and adjoint solution $(\mathbf{v}^*, q^*, \psi^*)$ satisfying (2.10) and (3.15) are inserted into (A.4) resulting in

$$
\mathcal{L}(\mathbf{u}^*, p^*; \mathbf{v}^*, q^*; h^*, \psi^*; b, C_\gamma, C) = \int_0^T \int_\omega F(\mathbf{u}^*, h^*)\,\mathrm{d}\mathbf{x}\,\mathrm{d}t. \tag{A.13}
$$

Then (A.12) yields the variation in $\mathcal{L}$ in (A.13) with respect to perturbations $\delta b, \delta C_\gamma$, and δC in b, C_γ, and C

$$
\begin{aligned}
\delta\mathcal{L} &= \int_0^T \int_\omega (2\eta\mathbf{D}(\mathbf{v}^*) : \mathbf{B}(\mathbf{u}^*) + \rho g\nabla h^*\cdot\mathbf{v}^* + \mathbf{u}^*\cdot\nabla\psi^*)\delta b\,\mathrm{d}\mathbf{x}\,\mathrm{d}t \\
&\quad - \int_0^T \int_{\gamma_g} \delta C_\gamma f_\gamma(\mathbf{t}\cdot\mathbf{u}^*)\mathbf{t}\cdot\mathbf{u}^*\,\mathbf{t}\cdot\mathbf{v}^*\,\mathrm{d}s\,\mathrm{d}t \\
&\quad - \int_0^T \int_\omega \delta C f(\mathbf{u}^*)\mathbf{v}^*\cdot\mathbf{u}^*\,\mathrm{d}\mathbf{x}\,\mathrm{d}t.
\end{aligned} \tag{A.14}
$$

A.3. Adjoint equations in FS. The FS Lagrangian is

$$
\begin{aligned}
&\mathcal{L}(\mathbf{u}, p, h; \mathbf{v}, q, \psi; C) = \int_0^T \int_{\Gamma_s} F(\mathbf{u}, h) + \psi(h_t + \mathbf{h}\cdot\mathbf{u} - a)\,dx\,\mathrm{d}t \\
&+ \int_0^T \int_\omega \int_b^h -\mathbf{v}\cdot(\nabla\cdot\boldsymbol{\sigma}(\mathbf{u}, p)) - q\nabla\cdot\mathbf{u} - \rho\mathbf{g}\cdot\mathbf{v}\;\mathrm{d}\mathbf{x}\,\mathrm{d}t \\
&= \int_0^T \int_{\Gamma_s} F(\mathbf{u}, h) + \psi(h_t + \mathbf{h}\cdot\mathbf{u} - a)\,\mathrm{d}\mathbf{x}\,\mathrm{d}t \\
&+ \int_0^T \int_\omega \int_b^h 2\eta(\mathbf{u})\mathbf{D}(\mathbf{v}) : \mathbf{D}(\mathbf{u}) - p\nabla\cdot\mathbf{v} - q\nabla\cdot\mathbf{u} - \rho\mathbf{g}\cdot\mathbf{v}\;\mathrm{d}\mathbf{x}\,\mathrm{d}t \\
&+ \int_0^T \int_{\Gamma_b} Cf(\mathbf{Tu})\mathbf{Tu}\cdot\mathbf{Tv}\,\mathrm{d}\mathbf{x}\,\mathrm{d}t.
\end{aligned} \tag{A.15}
$$

In the same manner as in (A.5), the perturbed FS Lagrangian is

$$
\begin{aligned}
&\mathcal{L}(\mathbf{u}+\delta\mathbf{u}, p+\delta p; \mathbf{v}+\delta\mathbf{v}, q+\delta q; h+\delta h, \psi+\delta\psi; C+\delta C) \\
&= \mathcal{L}(\mathbf{u}, p, h; \mathbf{v}, q, \psi; C) + I_1 + I_2 + I_3.
\end{aligned} \tag{A.16}
$$

Terms of order two or more in $\delta\mathbf{u}, \delta\mathbf{v}, \delta h$ are neglected. The first integral I_1 in (A.16) is

$$
\begin{aligned}
I_1 &= \int_0^T \int_{\Gamma_s} F(\mathbf{u}(\mathbf{x}, h+\delta h, t) + \delta\mathbf{u}, h+\delta h) - F(\mathbf{u}(\mathbf{x}, h, t), h)\,\mathrm{d}\mathbf{x}\,\mathrm{d}t \\
&= \int_0^T \int_{\Gamma_s} F_{\mathbf{u}}(\delta\mathbf{u} + \mathbf{u}_z\delta h) + F_h\delta h\,\mathrm{d}\mathbf{x}\,\mathrm{d}t.
\end{aligned} \tag{A.17}
$$

Partial integration, the conditions $\psi(\mathbf{x}, T) = 0$ and $\psi(\mathbf{x}, t) = 0$ at Γ_s, and the fact that h is a weak solution simplify the second integral

$$
\begin{aligned}
I_2 &= \int_0^T \int_{\Gamma_s} \delta\psi(h_t + \mathbf{h}\cdot\mathbf{u} - a) \\
&\quad + \psi(\delta h_t + \mathbf{u}\cdot\delta\mathbf{h} + \mathbf{u}_z\cdot\mathbf{h}\delta h + \mathbf{h}\cdot\delta\mathbf{u})\,\mathrm{d}\mathbf{x}\,\mathrm{d}t \\
&= \int_0^T \int_{\Gamma_s} \delta\psi(h_t + \mathbf{h}\cdot\mathbf{u} - a)\,\mathrm{d}\mathbf{x}\,\mathrm{d}t \\
&\quad + \int_0^T \int_{\Gamma_s} (-\psi_t - \nabla\cdot(\mathbf{u}\psi) + \mathbf{h}\cdot\mathbf{u}_z\psi)\delta h + \mathbf{h}\cdot\delta\mathbf{u}\psi\,\mathrm{d}\mathbf{x}\,\mathrm{d}t.
\end{aligned} \tag{A.18}
$$

Define Ξ, ξ, and Υ to be

$$\begin{aligned} \Theta(\mathbf{u},p;\mathbf{v},q;C) &= 2\eta(\mathbf{u})\mathbf{D}(\mathbf{v}):\mathbf{D}(\mathbf{u}) - p\nabla\cdot\mathbf{v} - q\nabla\cdot\mathbf{u} - \rho\mathbf{g}\cdot\mathbf{v}, \\ \theta(\mathbf{u};\mathbf{v};C) &= Cf(\mathbf{Tu})\mathbf{Tu}\cdot\mathbf{Tv}, \\ \Upsilon(\mathbf{u},p;\mathbf{v},q) &= -\mathbf{v}\cdot(\nabla\cdot\boldsymbol{\sigma}(\mathbf{u},p)) - q\nabla\cdot\mathbf{u} - \rho\mathbf{g}\cdot\mathbf{v}. \end{aligned} \tag{A.19}$$

Then a weak solution, $(\mathbf{u},p)$, for any $(\mathbf{v},q)$ satisfying the boundary conditions, fulfills

$$\int_0^T\int_\omega\int_b^h \Theta(\mathbf{u},p;\mathbf{v},q;C)\,\mathrm{d}\mathbf{x}\,\mathrm{d}t - \int_0^T\int_{\Gamma_b}\theta(\mathbf{u};\mathbf{v};C)\,\mathrm{d}\mathbf{x}\,\mathrm{d}t = 0. \tag{A.20}$$

The third integral in (A.16) is

$$\begin{aligned} I_3 = {} & I_{31} + I_{32}, \\ I_{31} = {} & \textstyle\int_0^T\int_\omega\int_b^h \Theta(\mathbf{u}+\delta\mathbf{u},p+\delta p;\mathbf{v}+\delta\mathbf{v},q+\delta q;C+\delta C)\,\mathrm{d}\mathbf{x}\,\mathrm{d}t \\ & \textstyle -\int_0^T\int_{\Gamma_b}\theta(\mathbf{u}+\delta\mathbf{u};\mathbf{v}+\delta\mathbf{v};C+\delta C)\,\mathrm{d}\mathbf{x}\,\mathrm{d}t, \\ I_{32} = {} & \textstyle\int_0^T\int_\omega\int_h^{h+\delta h}\Upsilon(\mathbf{u},p;\mathbf{v},q)\,\mathrm{d}\mathbf{x}\,\mathrm{d}t. \end{aligned} \tag{A.21}$$

The integral I_{31} is expanded as in (A.10) and (A.11) or [24] using the weak solution, Gauss' formula, and the definitions of the adjoint viscosity and adjoint friction coefficient in Section A.1. When $b < z < h$ we have $\Upsilon(\mathbf{u},p;\mathbf{v},q) = 0$. If Υ is extended smoothly in the positive z-direction from $z = h$, then with $z \in [h, h+\delta h]$ for some constant $c > 0$ we have $|\Upsilon| \le c\delta h$. Therefore,

$$\Big|\int_h^{h+\delta h(x,t)}\Upsilon(\mathbf{u},p;\mathbf{v},q)\,dz\Big| \le \int_h^{h+\delta h(x,t)}\sup|\Upsilon|\,dz \le c|\delta h(x,t)^2|,$$

and the bound on I_{32} in (A.21) is

$$|I_{32}| \le ct|\omega|\max|\delta h(x,t)|^2, \tag{A.22}$$

where $|\omega|$ is the area of ω. This term is a second variation in δh which is neglected and $I_3 = I_{31}$.

The first variation of $\mathcal{L}$ is then

$$\begin{aligned} \delta\mathcal{L} &= I_1 + I_2 + I_3 \\ &= \textstyle\int_0^T\int_{\Gamma_s}(F_\mathbf{u} + \psi\mathbf{h})\cdot\delta\mathbf{u}\,\mathrm{d}\mathbf{x}\,\mathrm{d}t \\ &\quad \textstyle + \int_0^T\int_{\Gamma_s}(F_h + F_\mathbf{u}\mathbf{u}_z - (\psi_t + \nabla\cdot(\mathbf{u}\psi) - \mathbf{h}\cdot\mathbf{u}\psi))\delta h\,\mathrm{d}\mathbf{x}\,\mathrm{d}t \\ &\quad \textstyle + \int_0^T\int_\omega\int_b^h 2\mathbf{D}(\mathbf{v}):(\tilde{\boldsymbol{\eta}}(\mathbf{u})\star\mathbf{D}(\delta\mathbf{u})) - \delta p\nabla\cdot\mathbf{v} - q\nabla\cdot\delta\mathbf{u}\,\mathrm{d}\mathbf{x}\,\mathrm{d}t \\ &\quad \textstyle + \int_0^T\int_{\Gamma_b} Cf(\mathbf{Tu})(\mathbf{I} + \mathbf{F}_b(\mathbf{u}))\mathbf{Tv}\cdot\mathbf{T}\delta\mathbf{u}\,\mathrm{d}\mathbf{x}\,\mathrm{d}t \\ &\quad \textstyle + \int_0^T\int_{\Gamma_b}\delta Cf(\mathbf{Tu})\,\mathbf{Tu}\cdot\mathbf{Tv}\,\mathrm{d}\mathbf{x}\,\mathrm{d}t. \end{aligned} \tag{A.23}$$

With the forward solution $(\mathbf{u}^*,p^*,h^*)$ and the adjoint solution $(\mathbf{v}^*,q^*,\psi^*)$ satisfying (2.5) and (3.2), the first variation with respect to perturbations δC in C is (cf. (A.14))

$$\delta\mathcal{L} = \int_0^T\int_{\Gamma_b} f(\mathbf{Tu}^*)\,\mathbf{Tu}^*\cdot\mathbf{Tv}^*\,\delta C\,\mathrm{d}\mathbf{x}\,\mathrm{d}t. \tag{A.24}$$

Appendix B. Simplified SSA equations.

The forward and adjoint SSA equations in (3.21) and (3.22) are solved analytically. The conclusion from the thickness equation in (3.21) is that

$$u(x)H(x) = u(0)H(0) + ax = ax, \tag{B.1}$$

since $u(0) = 0$. Solve the second equation in (3.21) for u on the bedrock with $x \le x_{GL}$ and insert into (B.1) using the assumptions for $x > 0$ that $b_x \ll H_x$ and $h_x \approx H_x$ to have

$$\frac{\rho g}{C} H^{m+1} H_x = \frac{\rho g}{C(m+2)} (H^{m+2})_x = -(ax)^m. \tag{B.2}$$

The equation for H^{m+2} for $x \le x_{GL}$ is integrated from x to x_{GL} such that

$$\begin{aligned} H(x) &= \left(H_{GL}^{m+2} + \frac{m+2}{m+1} \frac{Ca^m}{\rho g} (x_{GL}^{m+1} - x^{m+1}) \right)^{\frac{1}{m+2}}, \\ u(x) &= \frac{ax}{H}, \quad H_x = -\frac{Ca^m}{\rho g} \frac{x^m}{H^{m+1}}. \end{aligned} \tag{B.3}$$

For the floating ice at $x > x_{GL}$, $\rho g H h_x = 0$ implying that $h_x = 0$ and $H_x = 0$. Hence, $H(x) = H_{GL}$. The velocity increases linearly beyond the grounding line

$$u(x) = ax/H(x) = ax/H_{GL}, \ x > x_{GL}. \tag{B.4}$$

By including the viscosity term in (3.18) and assuming that $H(x)$ is linear in x, a more accurate formula is obtained for $u(x)$ on the floating ice in (6.77) of [6].

Appendix C. Jumps in ψ and v in SSA.

Multiply the first equation in (3.22) by H and the second equation by u to eliminate ψ_x. We get

$$-Cmu^m v - \rho g H^2 v_x = HF_h - uF_u. \tag{C.1}$$

Use the expression for u and H_x in (B.3). Then

$$\rho g H (mH_x v - H v_x) = HF_h - uF_u, \tag{C.2}$$

or equivalently

$$\left(\frac{v}{H^m} \right)_x = -\frac{1}{\rho g H^{m+2}} (HF_h - uF_u). \tag{C.3}$$

The solutions $\psi(x)$ and $v(x)$ of the adjoint SSA equation (3.19) have jumps at the observation point x_*. For x close to x_* in a short interval $[x_*^-, x_*^+]$ with $x_*^- < x_* < x_*^+$, integrate (C.3) to receive

$$\int_{x_*^-}^{x_*^+} \left(\frac{v}{H^m} \right)_x \mathrm{d}x = -\int_{x_*^-}^{x_*^+} \frac{HF_h - uF_u}{\rho g H^{m+2}} \mathrm{d}x. \tag{C.4}$$

Since H is continuous and u and v are bounded, when $x_*^- \to x_*^+$, then

$$v(x_*^+) - v(x_*^-) = -\frac{1}{\rho g H_*^2} \left(H_* \int_{x_*^-}^{x_*^+} F_h \, \mathrm{d}x - u_* \int_{x_*^-}^{x_*^+} F_u \, \mathrm{d}x \right). \tag{C.5}$$

A similar relation for ψ can be derived

$$\psi(x_*^+) - \psi(x_*^-) = \frac{1}{H_*} \int_{x_*^-}^{x_*^+} F_u \, \mathrm{d}x. \tag{C.6}$$

With $F_u = 0$ and $F_h = 0$ for $x < x_*$ and $v(0) = \psi_x(0) = 0$, we find that

$$v(x) = \psi_x(x) = 0, \quad \psi(x) = \psi(x_*^-), \ 0 \le x < x_*. \tag{C.7}$$

If $F(u,h) = u\delta(x - x_*)$, then by (C.5) and (C.6)

$$v(x_*^+) = \frac{u_*}{\rho g H_*^2}, \quad \psi(x_*^+) - \psi(x_*^-) = \frac{1}{H_*}, \tag{C.8}$$

and if $F(u,h) = h\delta(x - x_*)$, then

$$v(x_*^+) = -\frac{1}{\rho g H_*}, \quad , \psi(x_*^+) - \psi(x_*^-) = 0. \tag{C.9}$$

Appendix D. Analytical solutions in SSA.

By Appendix C, $v(x) = 0$ for $0 \le x < x_*$. Use equations in (3.22) with H_x in (B.3) for $x_* < x \le x_{GL}$ to have

$$\frac{v_x}{v} = -\frac{axCmu^{m-1}}{\rho g H^3} = -\frac{Cmu^m}{\rho g H^2} = \frac{mH_x}{H}.$$

Let $\mathcal{H}(x - x_*) = \int_{-\infty}^{x-x_*} \delta(s)\, ds$ be the Heaviside step function at x_*. Then

$$v(x) = C_v H(x)^m \mathcal{H}(x - x_*), \quad 0 \le x \le x_{GL}. \tag{D.1}$$

To satisfy the jump condition in (C.8) and (C.9), the constant C_v is

$$C_v = \begin{cases} \dfrac{ax_*}{\rho g H_*^{m+3}}, & F(u,h) = u\delta(x - x_*), \\ -\dfrac{1}{\rho g H_*^{m+1}}, & F(u,h) = h\delta(x - x_*). \end{cases} \tag{D.2}$$

Combine (D.1) with the relation $\psi_x = (F_u - Cmu^{m-1}v)/H$ and integrate from x to x_{GL} to obtain

$$\psi(x) = C_v a^{m-1} C \left(x_{GL}^m - x^m\right), \ x_* < x \le x_{GL}. \tag{D.3}$$

With the jump condition in (C.8) and (C.9), $\psi(x)$ at $0 \le x < x_*$ is

$$\psi(x) = \begin{cases} -\dfrac{1}{H_*} + \dfrac{Ca^m x_*}{\rho g H_*^{m+3}} \left(x_{GL}^m - x_*^m\right), & F(u,h) = u\delta(x - x_*), \\ -\dfrac{Ca^{m-1}}{\rho g H_*^{m+1}} (x_{GL}^m - x_*^m), & F(u,h) = h\delta(x - x_*). \end{cases} \tag{D.4}$$

The weight for δC in the functional $\delta\mathcal{L}$ in (3.20) is non-zero for $x_* < x \le x_{GL}$

$$-vu^m = -C_v (ax)^m. \tag{D.5}$$

Use (D.1) and (3.22) in (3.20) to determine the weight for δb in $\delta\mathcal{L}$,

$$\begin{aligned}\psi_x u + v_x \eta u_x + v\rho g h_x &= \rho g (Hv)_x + F_h \\ &= C_v \rho g H^m \left[(m+1) H_x \mathcal{H}(x - x_*) + H\delta(x - x_*)\right] + F_h.\end{aligned} \tag{D.6}$$

Acknowledgments. This work was supported by Nina Kirchner's Formas grant 2017-00665. Lina von Sydow read a draft of the paper and helped us improve the presentation with her comments.

REFERENCES

[1] J. Brondex, F. Gillet-Chaulet, and O. Gagliardini, *Sensitivity of centennial mass loss projections of the Amundsen basin to the friction law*, Cryosphere, 13 (2019), pp. 177–195.

[2] G. Cheng and P. Lötstedt, *Parameter sensitivity analysis of dynamic ice sheet models-Numerical computations*, arXiv e-prints, (2019), arXiv:1906.08209, https://arxiv.org/abs/1906.08209.

[3] O. Gagliardini, T. Zwinger, F. Gillet-Chaulet, G. Durand, L. Favier, B. de Fleurian, R. Greve, M. Malinen, C. Martín, P. Råback, J. Ruokolainen, M. Sacchettini, M. Schäfer, H. Seddik, and J. Thies, *Capabilities and performance of Elmer/Ice, a new generation ice-sheet model*, Geosci. Model Dev., 6 (2013), pp. 1299–1318.

[4] F. Gillet-Chaulet, G. Durand, O. Gagliardini, C. Mosbeux, J. Mouginot, F. Rémy, and C. Ritz, *Assimilation of surface velocities acquired between 1996 and 2010 to constrain the form of the basal friction law under Pine Island Glacier*, Geophys. Res. Lett., 43 (2016), pp. 10311–10321.

[5] J. W. Glen, *The creep of polycrystalline ice*, Proceedings of the Royal Society of London. Series A. Mathematical and Physical Sciences, 228 (1955), pp. 519–538.

[6] R. Greve and H. Blatter, *Dynamics of Ice Sheets and Glaciers*, Advances in Geophysical and Environmental Mechanics and Mathematics (AGEM^2), Springer, Berlin, 2009.

[7] G. H. Gudmundsson, *Transmission of basal variability to glacier surface*, J. Geophys. Res., 108 (2003).

[8] G. H. Gudmundsson, *Analytical solutions for the surface response to small amplitude perturbations in boundary data in the shallow-ice-stream approximation*, Cryosphere, 2 (2008), pp. 77–93.

[9] G. H. Gudmundsson and M. Raymond, *On the limit to resolution and information on basal properties obtainable from surface data on ice streams*, Cryosphere, 2 (2008), pp. 167–178.

[10] P. Heimbach and M. Losch, *Adjoint sensitivities of sub-ice-shelf melt rates to ocean circulation under the Pine Island Ice Shelf, West Antarctica*, Ann. Glaciol., 53 (2012), pp. 59–69.

[11] K. Hutter, *Theoretical Glaciology*, D. Reidel Publishing Company, Terra Scientific Publishing Company, Dordrecht, 1983.

[12] T. Isaac, N. Petra, G. Stadler, and O. Ghattas, *Scalable and efficient algorithms for the propagation of uncertainty from data through inference to prediction for large-scale problems with application to flow of the Antarctic ice sheet*, J. Comput. Phys., 296 (2015), pp. 348–368.

[13] M. Jay-Allemand, F. Gillet-Chaulet, O. Gagliardini, and M. Nodet, *Investigating changes in basal conditions of Variegated Glacier prior to and during its 1982-1983 surge*, Cryosphere, 5 (2011), pp. 659–672.

[14] T. M. Kyrke-Smith, G. H. Gudmundsson, and P. E. Farrell, *Relevance of detail in basal topography for basal slipperiness inversions: a case study on Pine Island Glacier, Antarctica*, Frontiers Earth Sci., 6 (2018), p. 33.

[15] D. R. MacAyeal, *Large-scale ice flow over a viscous basal sediment: Theory and application to Ice Stream B, Antarctica.*, J. Geophys. Res., 94 (1989), pp. 4071–4078.

[16] D. R. MacAyeal, *A tutorial on the use of control methods in ice sheet modeling*, J. Glaciol., 39 (1993), pp. 91–98.

[17] N. Martin and J. Monnier, *Adjoint accuracy for the full Stokes ice flow model: limits to the transmission of basal friction variability to the surface*, Cryosphere, 8 (2014), pp. 721–741.

[18] B. Minchew, M. Simons, H. Björnsson, F. Pálsson, M. Morlighem, H. Seroussi, E. Larour, and S. Hensley, *Plastic bed beneath Hofsjökull Ice Cap, central Iceland, and the sensitivity of ice flow to surface meltwater flux*, J. Glaciol., 62 (2016), pp. 147–158.

[19] B. M. Minchew, C. R. Meyer, S. S. Pegler, B. P. Lipovsky, A. W. Rempel, G. H. Gudmundsson, and N. R. Iverson, *Comment on "Friction at the bed does not control fast glacier flow"*, Science, 363 (2019), p. eaau6055.
[20] L. W. Morland, *Thermo–mechanical balances of ice sheet flows*, Geophys. Astrophys. Fluid Dynam., 29 (1984), pp. 237–266.
[21] M. Morlighem, H. Seroussi, E. Larour, and E. Rignot, *Inversion of basal friction in Antarctica using exact and incomplete adjoints of a high-order model*, J. Geophys. Res.: Earth Surf., 118 (2013), pp. 1–8.
[22] W. J. J. van Pelt, J. Oerlemans, C. H. Reijmer, R. Pettersson, V. A. Pohjola, E. Isaksson, and D. Divine, *An iterative inverse method to estimate basal topography and initialize ice flow models*, Cryosphere, 7 (2013), pp. 987–1006.
[23] M. Perego, S. F. Price, and G. Stadler, *Optimal initial conditions for coupling ice sheet models to Earth system models*, J. Geophys. Res. Earth Surf., 119 (2014), pp. 1894–1917.
[24] N. Petra, H. Zhu, G. Stadler, T. J. R. Hughes, and O. Ghattas, *An inexact Gauss-Newton method for inversion of basal sliding and rheology parameters in a nonlinear Stokes ice sheet model*, J. Glaciol., 58 (2012), pp. 889–903.
[25] C. Ritz, T. L. Edwards, G. Durand, A. J. Payne, V. Peyaud, and R. C. Hindmarsh, *Potential sea level rise from Antarctic ice-sheet instability constrained by observations*, Nature, 528 (2015), pp. 115–118.
[26] C. Schannwell, R. Drews, T. A. Ehlers, O. Eisen, C. Mayer, and F. Gillet-Chaulet, *Kinematic response of ice-rise divides to changes in oceanic and atmospheric forcing*, Cryosphere Discuss., (2019).
[27] C. Schoof, *Ice sheet grounding line dynamics: Steady states, stability and hysteresis*, J. Geophys. Res.: Earth Surf., 112 (2007), p. F03S28.
[28] C. Schoof, *Ice-sheet acceleration driven by melt supply variability*, Nature, 468 (2010), pp. 803–806.
[29] O. Sergienko and R. C. A. Hindmarsh, *Regular patterns in frictional resistance of ice-stream beds seen by surface data inversion*, Science, 342 (2013), pp. 1086–1089.
[30] A. J. Sole, D. W. F. Mair, P. W. Nienow, I. D. Bartholomew, I. D. King, M. A. Burke, and I. Joughin, *Seasonal speedup of a Greenland marine-terminating outlet glacier forced by surface melt-induced changes in subglacial hydrology*, J. Geophys. Res., 116 (2011), p. F03014.
[31] L. A. Stearn and C. J. van der Veen, *Friction at the bed does not control fast glacier flow*, Science, 361 (2018), pp. 273–277.
[32] T. Thorsteinsson, C. F. Raymond, G. H. Gudmundsson, R. A. Bindschadler, P. Vornberger, and I. Joughin, *Bed topography and lubrication inferred from surface measurements on fast-flowing ice streams*, J. Glaciol., 49 (2003), pp. 481–490.
[33] V. C. Tsai, A. L. Stewart, and A. F. Thompson, *Marine ice-sheet profiles and stability under coulomb basal conditions*, Journal of Glaciology, 61 (2015), pp. 205–215.
[34] D. Vallot, R. Pettersson, A. Luckman, D. I. Benn, T. Zwinger, W. J. J. van Pelt, J. Kohler, M. Schäfer, B. Claremar, and N. R. J. Hulton, *Basal dynamics of Kronebreen, a fast-flowing tidewater glacier in Svalbard: non-local spatio-temporal response to water input*, J. Glaciol., 11 (2017), pp. 179–190.
[35] C. J. van der Veen, *Tidewater calving*, J. Glaciol., 42 (1996), pp. 375–385.
[36] J. Weertman, *On the sliding of glaciers*, J. Glaciol., 3 (1957), pp. 33–38.
[37] M. Weis, R. Greve, and K. Hutter, *Theory of shallow ice shelves*, Continuum Mech. Thermodyn., 11 (1999), pp. 15–50.
[38] H. Yu, E. Rignot, H. Seroussi, and M. Morlighem, *Retreat of Thwaites Glacier, West Antarctica, over the next 100 years using various ice flow models, ice shelf melt scenarios and basal friction laws*, Cryosphere, 12 (2018), pp. 3861–3876.